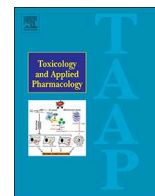




Since January 2020 Elsevier has created a COVID-19 resource centre with free information in English and Mandarin on the novel coronavirus COVID-19. The COVID-19 resource centre is hosted on Elsevier Connect, the company's public news and information website.

Elsevier hereby grants permission to make all its COVID-19-related research that is available on the COVID-19 resource centre - including this research content - immediately available in PubMed Central and other publicly funded repositories, such as the WHO COVID database with rights for unrestricted research re-use and analyses in any form or by any means with acknowledgement of the original source. These permissions are granted for free by Elsevier for as long as the COVID-19 resource centre remains active.



Formation of lamellar body-like structure may be an initiator of didecyldimethylammonium chloride-induced toxic response



Eun-Jung Park^{a,*}, Eunsol Seong^{a,1}, Min-Sung Kang^b, Gwang-Hee Lee^c, Dong-Wan Kim^c, Ji-Seok Han^d, Hyun-Ji Lim^a, Seung Hyeun Lee^e, Hyoung-Yun Han^f

^a East-West Medical Science Research Institute, Kyung Hee University, Seoul 02447, Republic of Korea

^b In vivo Hazard Evaluation & Research Division, General Toxicology & Research Group, Jeonbuk Branch Institute, Korea Institute of Toxicology, Jeongeup-si, Jeollabuk-do, Republic of Korea

^c School of Civil, Environmental, Architectural Engineering, Korea University, Seoul 136-713, Republic of Korea

^d Department of Advanced Toxicology Research, Korea Institute of Toxicology, 141 Gajeong-ro, Yuseong-gu, Daejeon, Republic of Korea

^e Division of Pulmonary and Critical Care Medicine, Department of Internal Medicine, School of Medicine, Kyung Hee University, Seoul 02447, Republic of Korea

^f Department of Predictive Toxicology, Korea Institute of Toxicology, Daejeon 34114, Republic of Korea

ARTICLE INFO

Keywords:

Didecyldimethylammonium chloride
Disinfectants
Quaternary ammonium compounds
Lamella body
Matrix metalloproteinase-1
Idiopathic pulmonary fibrosis

ABSTRACT

Due to the pandemic of coronavirus disease 2019, the use of disinfectants is rapidly increasing worldwide. Didecyldimethylammonium chloride (DDAC) is an EPA-registered disinfectant, it was also a component in humidifier disinfectants that had caused idiopathic pulmonary diseases in Korea. In this study, we identified the possible pulmonary toxic response and mechanism using human bronchial epithelial (BEAS-2B) cells and mice. First, cell viability decreased sharply at a 4 µg/mL of concentration. The volume of intracellular organelles and the ROS level reduced, leading to the formation of apoptotic bodies and an increase of the LDH release. Secretion of pro-inflammatory cytokines (IL-1β, IL-6, and TNF-α) and matrix metalloproteinase-1 also significantly increased. More importantly, lamellar body-like structures were formed in both the cells and mice exposed to DDAC, and the expression of both the indicator proteins for lamellar body (ABCA3 and Rab11a) and surfactant proteins (A, B, and D) was clearly enhanced. In addition, chronic fibrotic pulmonary lesions were notably observed in mice instilled twice (weekly) with DDAC (500 µg), ultimately resulting in death. Taken together, we suggest that disruption of pulmonary surfactant homeostasis may contribute to DDAC-induced cell death and subsequent pathophysiology and that the formation of lamellar body-like structures may play a role as the trigger. In addition, we propose that the cause of sudden death of mice exposed to DDAC should be clearly elucidated for the safe application of DDAC.

1. Introduction

Needless to say, traffic jams, chimney smoke from factories and homes, and dirt from construction sites are typical sources of air pollution. However, it can be said that the source of air pollution is more complex and diverse than we can imagine, and the use of cleaning products, such as laundry detergents, bleaches, dishwashing products and other household cleaners has been raised as one of them. In addition, release of disinfectants into the atmosphere is rapidly increasing due to the coronavirus disease 2019 (COVID-19) pandemic.

Quaternary-ammonium compounds (QACs) are salts of quaternary-ammonium cations and contain one quaternary nitrogen covalently substituted with four alkyl or aryl residues (Gilbert and Moore, 2005).

QACs also show positive charge which can bind strongly to cell walls and membranes of microorganisms, and QACs containing long alkyl chains can induce fatal damage to a wide variety of organisms such as fungi, amoebas and enveloped viruses by disrupting their membranes (Gerba, 2015; Hegstad et al., 2010). Therefore, QACs have been employed in daily products such as disinfectants, surfactants, softeners, and shampoos, they have also been used in the food-processing industry as antiseptics and in clinics as antibiotics (Zhang et al., 2015).

Didecyldimethylammonium chloride (DDAC) is a representative QAC that is registered on the US EPA Office of Pesticide Programs (U.S. EPA, 2005). It has been widely used as an antiseptic, disinfectant, and antibiotic to prevent proliferation of microorganisms in commercial and residential applications such as wood and construction supplies, water

* Corresponding author at: East-West Medical Science Research Institute, Kyung Hee University, Kyung Hee Daero 23, Dongdaemun-gu, Seoul 02447, Republic of Korea.

E-mail address: pejtoxic@khu.ac.kr (E.-J. Park).

¹ These authors contributed equally to this work as first authors.

<https://doi.org/10.1016/j.taap.2020.115182>

Received 22 July 2020; Accepted 30 July 2020

Available online 05 August 2020

0041-008X/© 2020 Elsevier Inc. All rights reserved.

tanks, humidifiers and laundries (Pubchem, 2005; Consumer Product Information Database, 2020), it has been also recommended for the sterilization of swimming pools, milking equipment, udders, and surgical instruments (U.S.EPA, 2006).

Meanwhile, the number of patients with irreversible lung injury increased rapidly in Korea since 2006. Epidemiological and toxicological studies have demonstrated humidifier disinfectants containing biocidal ingredients as the cause and polyhexamethylene guanidine phosphate (PHMG-P), Kathon (a mixture of methylisothiazolinone and chloromethylisothiazolinone), and DDAC as the main ingredients (Lee et al., 2012; Kim et al., 2014; Leem and Lee, 2017). Thus, sales of humidifier disinfectants containing these chemicals were legally prohibited in the Korean market. However, other types of products containing these compounds (or derivatives) are still on the global markets. Increasing evidence has also suggested that these ingredients induce different toxic mechanism and subsequent pathologies, ultimately leading to different diseases and that the toxic mechanism depends on how the compounds interact with the biological systems. Meanwhile, with regard to DDAC-associated toxicity, there are controversial reports. For example, Kim et al. (2017) published that significant histopathological lesions were not found in rats after inhalation at a concentration of 0.11 mg/m³ for 13 weeks. Other researchers have shown that DDAC strongly binds to negatively charged lipid bilayers and leads to dissociation of the cell-membrane components and leakage of intracellular components, resulting in cell death (Yoshimatsu and Hiyama, 2007; Jansen et al., 2013). In addition, ambient exposure to DDAC combined with alkyldimethylbenzyl ammonium chloride led to neural tube defects that persisted for two generations after cessation of exposure (Hrubec et al., 2017). Herein, we aimed to identify the possible pulmonary toxic response and the mechanism of inhaled DDAC using mice and human bronchial epithelial cells (BEAS-2B cells).

2. Materials and methods

2.1. Cell culture and DDAC characterization

BEAS-2B cells (American Type Culture Collection, VA, USA) were maintained in DMEM/F12 medium containing 10% fetal bovine serum (FBS) and 1% penicillin-streptomycin (Corning, NY, USA) at 37 °C and 5% CO₂/95% O₂, and DDAC (Sigma-Aldrich, MO, USA) was dissolved in distilled water (DW, 1 mg/mL) and serially diluted prior to treatment. Cells treated with DW of the same volume were used as the control. In addition, morphology of DDAC suspended in DW was characterized by transmission electron microscopy (TEM, JEOL, JEM-2100F, Japan), and the surface charge and particle size were characterized using a zeta potential analyzer (ELSZ-1000, Photal Otsuka Electronics).

2.2. Cell viability

BEAS-2B cells (2×10^4 cells/mL) were stabilized overnight in a 96-well plate, and the cells were treated with the designated concentration of DDAC. After 24 h incubation, the media were replaced with FBS-free culture media containing 3-(4,5-dimethylthiazol-2-yl)-2,5-diphenyltetrazolium bromide (20 µg/mL) and further incubated for 4 h at 37 °C. After removing the supernatants, purple formazan was dissolved in dimethyl sulfoxide, and the absorbance was measured at 540 nm using a UV spectrophotometer (ParkinElmer, MA, USA).

2.3. Effects on the cell membrane

According to the manufacturer's instructions (ThermoFisher Scientific, Waltham, MA, USA), the cells (2×10^5 cells/mL) were incubated in media containing DDAC for 24 h. A part of the cell supernatant was reacted with the LDH reaction mixture (1:1) in a new 96-

well plate for 30 min at room temperature (RT). The absorbance was quantified at 490 nm using a UV spectrophotometer (ParkinElmer).

2.4. Observation of cell morphology

First, stabilized cells (70% - 80% confluence) were incubated with or without DDAC (2 or 4 µg/mL) for 24 h. Cell morphology was examined using a phase contrast microscope coupled with a microscope-image-detector module (CKX53, Olympus, Shinjuku, Tokyo, Japan; eXcope T500, DIXI Science, Daejeon, Korea). Additionally, both the cells and lung tissues of mice exposed to DDAC were fixed in Karnovsky's fixative solution overnight. After washing with 0.05 M sodium cacodylate buffer, the samples were re-fixed in 2% osmium tetroxide and 0.1 M cacodylate buffer (1:1) for 2 h and stained with 0.5% uranyl acetate. The samples were then dehydrated using serially diluted ethanol solutions (30%, 50%, 70%, 80%, 90%, and 100%) and propylene oxide, and subsequently embedded in Spurr's resin. Finally, the internal structures were observed under an 80-kV transmission electron microscope (TEM, LIBRA 120, Carl Zeiss, Oberkochen, Germany).

2.5. Integrity of intracellular components

Stabilized cells (70% - 80% confluence) were exposed to DDAC (0, 1, 2, and 4 µg/mL) for 24 h, the cells were further incubated in culture media containing MitoTracker Green FM (150 nM, for mitochondrial volume), MitoTracker Red CMXRos (200 nM, for mitochondrial membrane potential), ER Tracker Green (250 nM, for the endoplasmic reticulum [ER] volume), LysoTracker Green (50 nM, for lysosomal volume), or Rhod-2 AM (1 µM, for mitochondrial calcium ion) according to the manufacturer's instructions (ThermoFisher Scientific, Puleston, 2015). The intracellular fluorescence level was assessed using flow cytometry (FACSaria III, BD Biosciences).

2.6. Identification of apoptotic cell death

Considering morphological changes observed in cells, we examined the effect of DDAC on the formation of apoptotic bodies. After 24 h incubation with DDAC (0, 1, 2, and 4 µg/mL), total cells were suspended in annexin-V binding buffer according to the manufacturer's instructions (Biolegend, CA, USA), and the cells were reacted with annexin V and propidium iodide (PI). Additionally, to test whether changes in cell cycle is involved in the process of DDAC-induced apoptotic cell death, the cells put overnight in 70% ethanol at -20 °C and then reacted with PI (20 µg/mL) and RNase (200 µg/mL, Sigma-Aldrich) for 15 min at RT. The formation of apoptotic bodies and the changes in cell cycle were identified using flow cytometry (BD Biosciences).

2.7. Levels of intracellular free radicals

At 24 h after exposure to DDAC (0, 1, 2, and 4 µg/mL), the cells were further incubated in FBS-free culture media containing carboxy-2, 7' dichlorofluorescein-diacetate (DCFH-DA, 20 µM, ThermoFisher Scientific, MA, USA), an indicator of reactive oxygen species (ROS), for 30 min at 37 °C. The intracellular ROS level was evaluated by measuring the fluorescence intensity at 488 nm using flow cytometry (BD Biosciences). In addition, effect of DDAC on the production of nitric oxide (NO), a common progenitor of reactive nitrogen species (RNS) was evaluated using a commercial Griess reagent kit (Biovision, CA, USA). Briefly, cells (1×10^6 cells/mL) were incubated with or without DDAC for 24 h, and the supernatants were reacted with the NO detection solution according to the manufacturer's instructions. The NO level was evaluated by measuring the absorbance at 540 nm using a microplate reader (PerkinElmer).

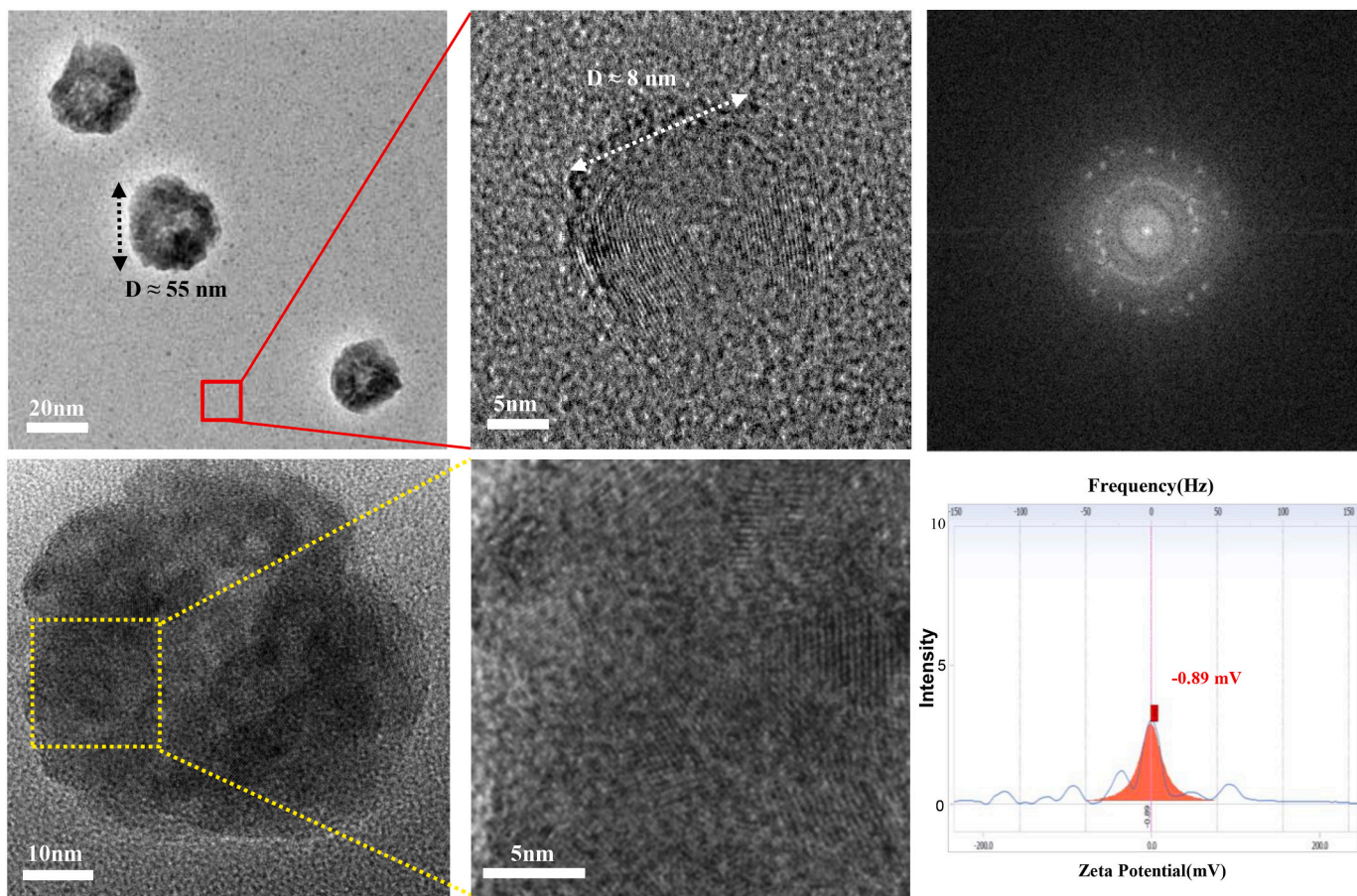


Fig. 1. Characterization of DDAC in DW. High-magnification TEM image of small DDAC (upper) and large DDAC (below) suspended in DW.

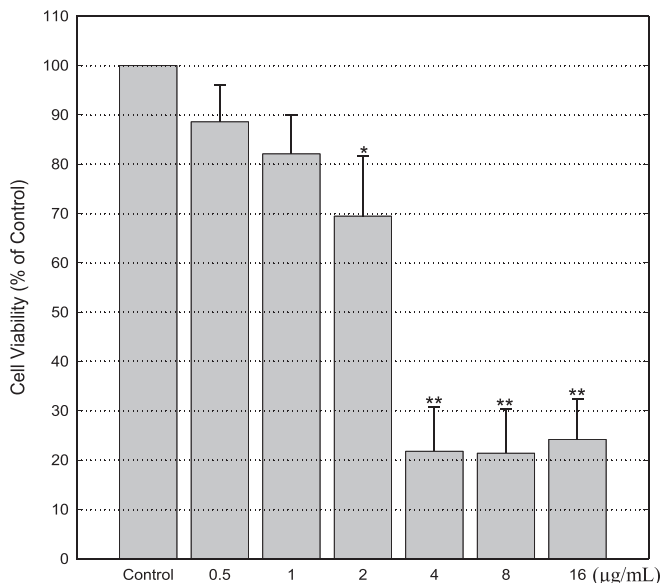


Fig. 2. Decrease in cell viability. Cells (2000 cells/well) were seeded in a 96-well plate and stabilized overnight. The cells were exposed to DDAC for 24 h, and the viability was presented as the mean ± standard deviation (SD) of four independent experiments (N = 4).

2.8. Gene profile analysis

BEAS-2B cells were incubated with or without 4 µg/mL of DDAC for 24 h and investigated changes in gene profile using microarray analysis technique. Briefly, mRNA preparation and microarray analysis were performed in Macrogen (Seoul, Korea) using Affymetrix Human 2.0 ST genechip according to the manufacturer's instructions (Illumina, Inc., San Diego, USA). The data were summarized and normalized with robust multi-average (RMA) method implemented in Affymetrix® Power Tools (APT). We exported the result with gene level RMA analysis and performed the differentially expressed gene analysis. Statistical significance of the expression data was determined using fold change. For a DEG set, Hierarchical cluster analysis was conducted using complete linkage and Euclidean distance as a measure of similarity. Gene-Enrichment and Functional Annotation analysis for significant probe list were done using Gene Ontology (<http://geneontology.org>) and KEGG (www.genome.jp/kegg/). All data analysis and visualization of differentially expressed genes were performed using R 3.3.3 (www.r-project.org).

2.9. Protein expression

The cells were harvested at 24 h after DDAC exposure (0, 1, 2, and 4 µg/mL) and lysed in protein extraction solution (PRO-PREP™, iNtRON Biotechnology, Seongnam-si, Kyunggi-do, Korea). After centrifugation at 13,000 rpm for 30 min, the amount of protein in the lysates was quantified by bicinchoninic acid assay (Sigma-Aldrich), and the same amounts of

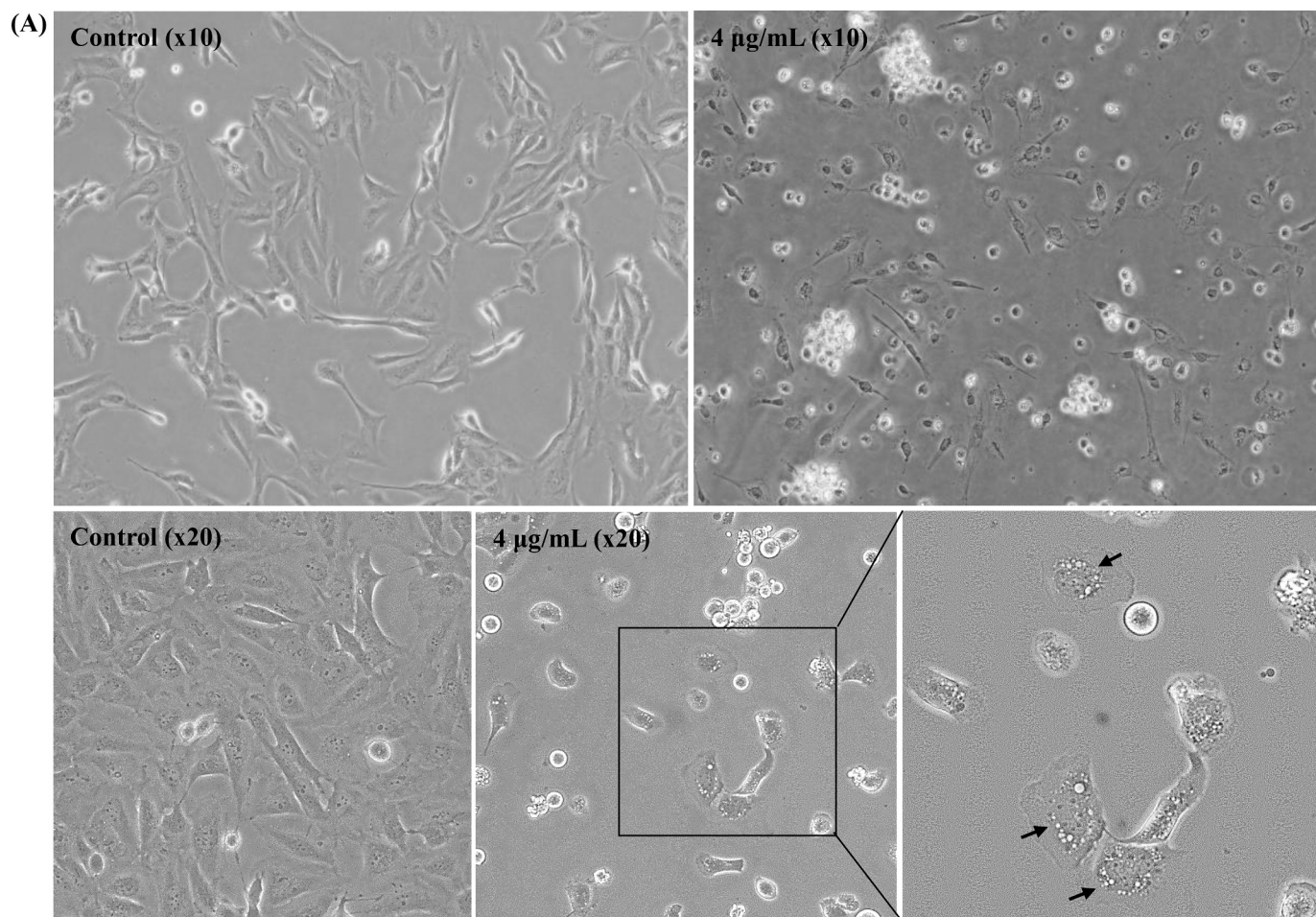


Fig. 3. Morphological changes.

(A) Phase-contrast images. Cells were incubated with or without DDAC for 24 h. Black arrows indicate the formation of vacuoles following DDAC exposure. TEM images were made using BEAS-2B cells exposed to 2 µg/mL (B) and 4 µg/mL (C) of DDAC for 24 h. We can show formation of lamellar body-like structures, and black arrows indicate damage the nuclear membrane.

proteins were loaded onto an SDS polyacrylamide gel (12%). Then, the proteins were transferred to nitrocellulose membranes (0.45 µm pore, GE Healthcare Life Sciences, Freiburg, Baden-Württemberg, Germany) and blocked with 5% skim milk in PBS containing 0.05% Tween-20 (PBST). The membranes were incubated overnight at 4 °C with the following primary antibodies; mouse monoclonal antibody for epidermal-growth-factor receptor (EGFR), vacuolar-type H⁺-ATPase (V-ATPase), lysosome-associated membrane protein (LAMP-2), β-Actin, surfactant proteins (SP)-A, SP-B, SP-D, chloride intracellular channel (CLIC)1, CLIC4 (Santa Cruz Biotechnology, Dallas, TX, USA), p62 and mitofusin (MFN)1 (Abcam, Cambridge, UK), rabbit polyclonal antibody for ATP-binding cassette A3 (ABCA3, Abcam), caspase-3, poly (ADP-ribose) polymerase (PARP), Rab11b, p-p53, and microtubule-associated proteins 1A/1B light chain (LC) 3B (Cell Signaling, Danvers, MA, USA), rabbit monoclonal antibody for dynamin-like 120 kDa protein, mitochondrial (OPA1, Abcam), and goat polyclonal antibody for apoptotic-protease activating factor (Apaf)-1 (Santa Cruz Biotechnology). Then, the reactants were reacted with HRP-conjugated secondary antibodies (Santa Cruz) and blotted using a ChemiDoc XRS+ system (Bio-Rad Laboratories Inc., Hercules, CA, USA). The cells were also stabilized on cover glass (18 mmØ, Marienfeld, Am Wöllerspfad, Lauda-Königshofen, Germany) and incubated with or without DDAC (4 µg/mL) for 24 h. The cells were fixed in 4% paraformaldehyde followed by 100% methanol and blocked with 3% bovine serum albumin in PBST. In

addition, the cells (1×10^6 cells/mL) were incubated with DDAC in a 12-well plate for 24 h. The levels of soluble proteins [Interleukin (IL)-1β, Tumor necrosis factor alpha (TNF-α), IL-6, transforming growth factor (TGF)-β chemokine (C-X-C motif) ligand (CXCL)8 (eBioscience, San Diego, CA, USA), CXCL1, and matrix metalloproteinase (MMP)-1 and 3 (R&D Systems, Minneapolis, MN, USA)] in the cell supernatants and BAL fluids were measured using commercial enzyme-linked immunosorbent assay kits. Finally, the absorbance was measured at 450 nm using a UV spectrophotometer (ParkinElmer), and the concentration of each protein was calculated using a standard curve generated under the same conditions.

2.10. Acute toxic response of DDAC in mice

Male ICR mice (6-week-old) were purchased from Orient-Bio Animal Company (Seongnam, Gyeonggi-do, South Korea) and acclimated for 10 days in our facility at 23 ± 1 °C, $55 \pm 5\%$ of humidity and dark/light cycle with interval of 12 h. The mice (32.5 ± 1.9 g) were anesthetized by inhalation of isoflurane (Hana Pharm. Co. Ltd., Hwaseong-si, Gyeonggi-do, South Korea) and nitrous gas, and DDAC (2000, 1000, 500, 250, and 125 µg/50 µL/mouse, three mice/dose) was instilled intratracheally to decide the acute pulmonary toxicity level. Control group was treated with DW of the same volume. While all mice treated with 2000 and 1000 µg died within 24 h after a single

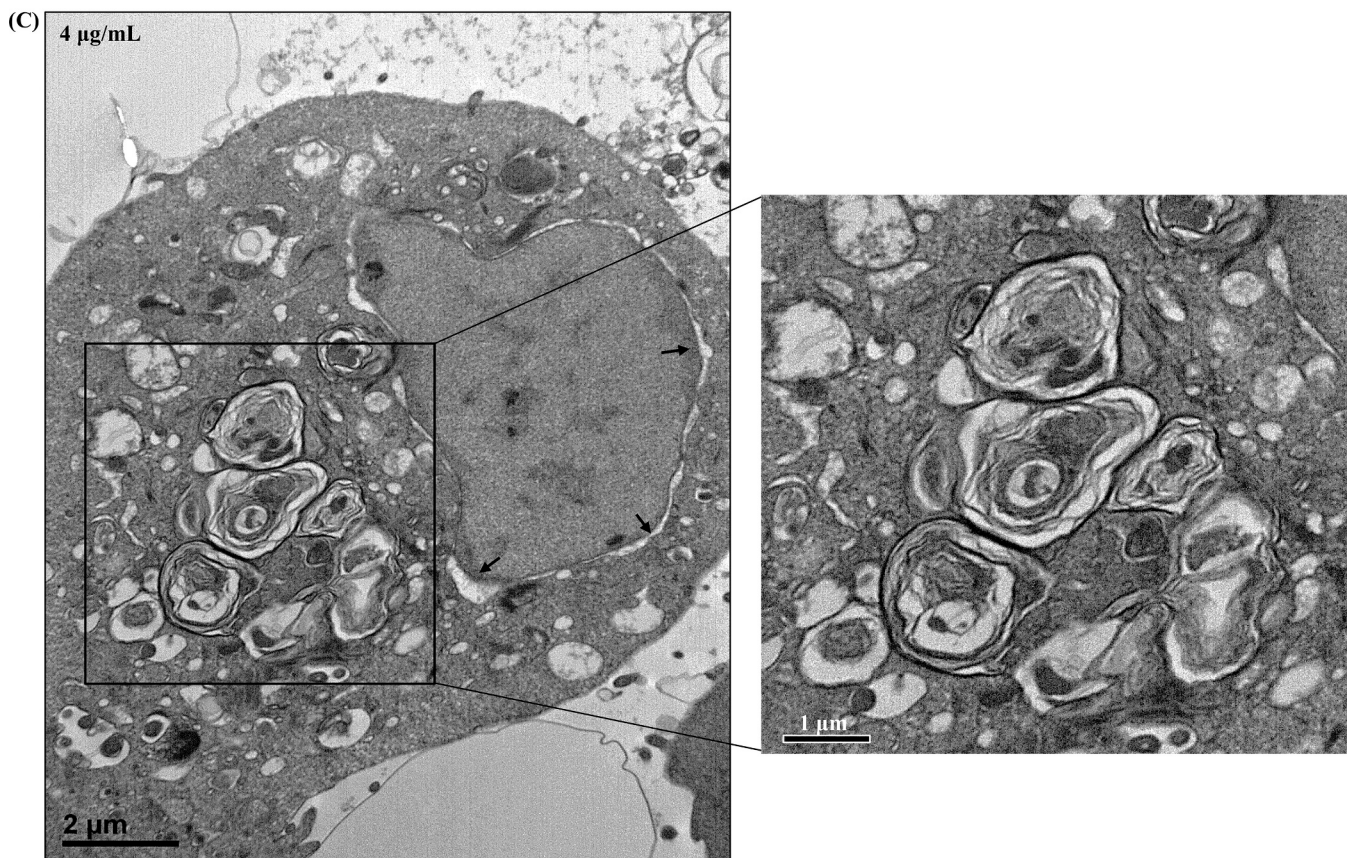
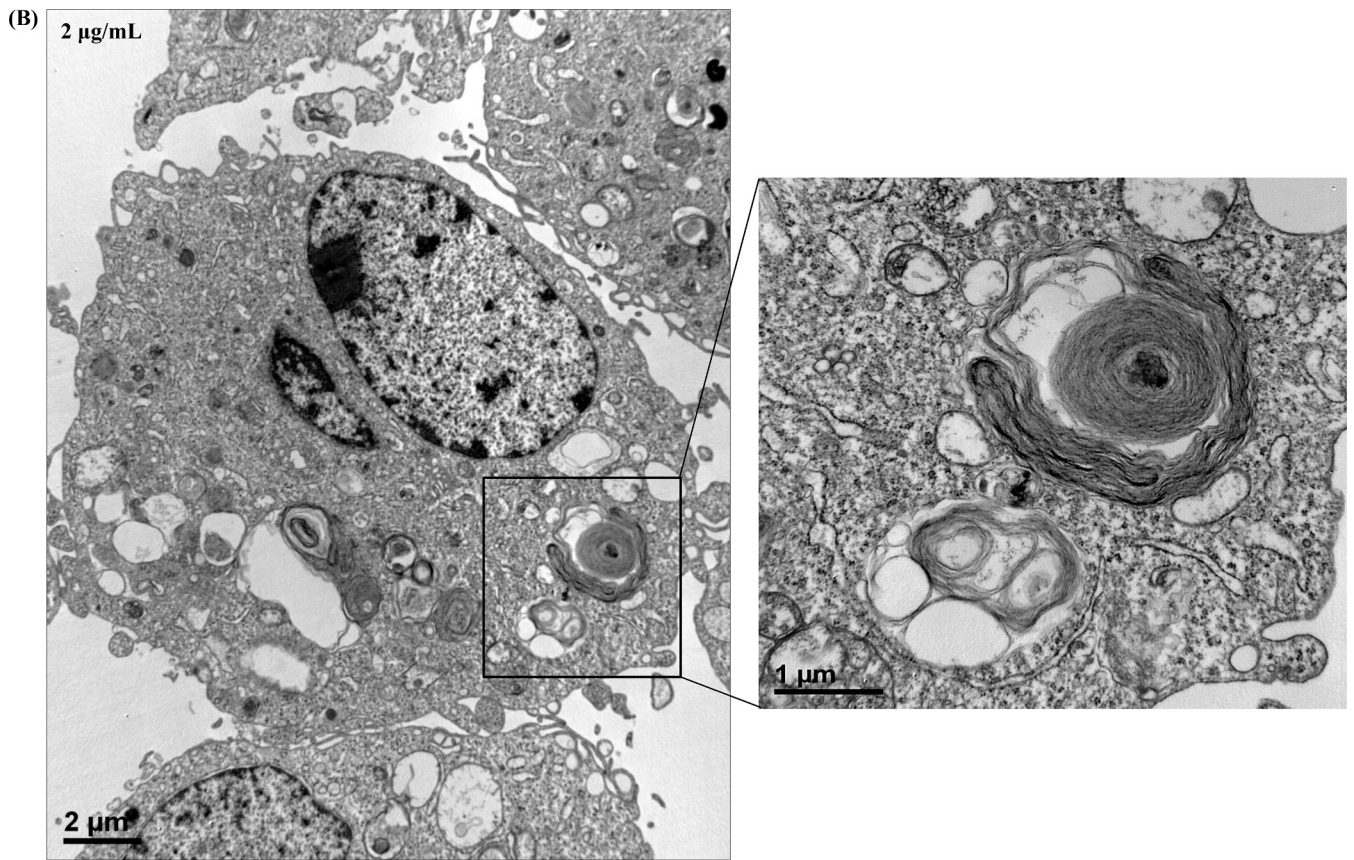


Fig. 3. (continued)

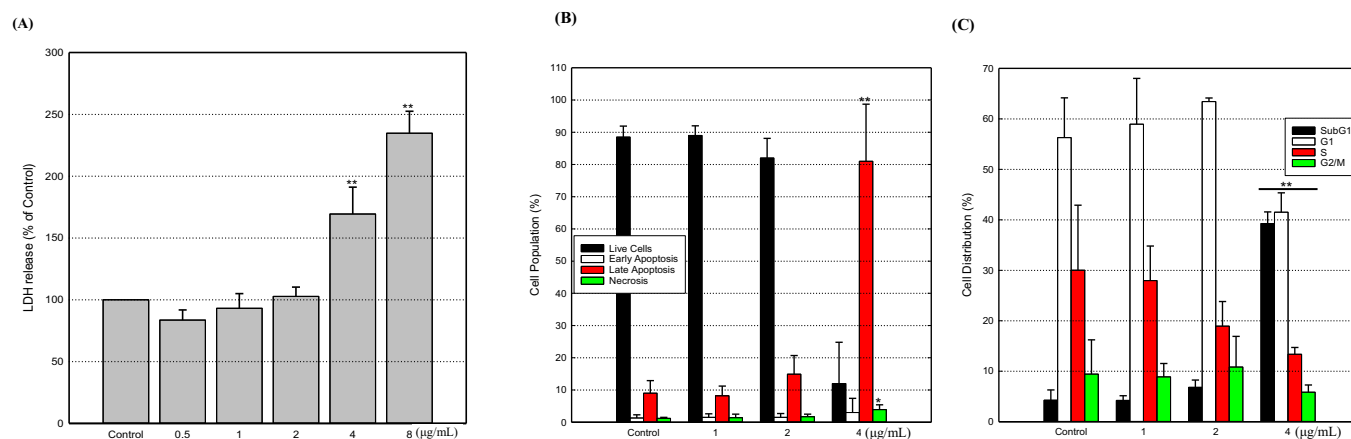


Fig. 4. Identification of cell death pathway.

(A) Increased LDH release. Cells (20,000 cells/well) were incubated with DDAC for 24 h, and a part (10 µL) of the supernatants was used to evaluate the LDH concentration. The experiment was independently performed four times ($N = 4$). Identification of apoptotic cell death (B) and changes in cell cycle (C) were performed using a FACS system. At 24 h after DDAC treatment (0, 1, 2, or 4 µg/mL), total cells were harvested and divided into two fractions for apoptotic cell death identification and cell cycle analysis. All experiments were independently performed three times ($N = 3$), and 10,000 cells per sample were analyzed by a FACS system. * $p < 0.05$, ** $p < 0.01$.

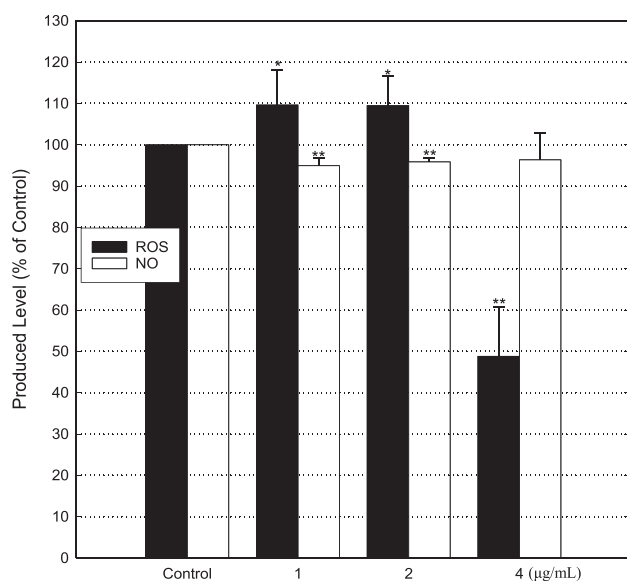


Fig. 5. Generation of free radicals.

Stabilized cells were incubated in 6-well plates with or without DDAC for 24 h, and the cells were then incubated with DCFH-DA for 4 h in a CO_2 incubator to evaluate intracellular ROS levels. The attached cells were harvested, and the intracellular fluorescent intensity (10,000 cells/sample) was measured using FACS system. In addition, BEAS-2B cells (1×10^6 cells/mL) were incubated with or without DDAC for 24 h in 96-well plates, and the supernatants were reacted with NO detection solution. Both experiments were independently performed three times ($N = 3$).

instillation, all the mice treated at concentrations below 500 µg survived up to 14 days. Following, we repeatedly instilled DDAC to mice at a 500, 250 and 125 µg of dose to identify a cause of death (male and female, 12 mice/sex/dose, one time per week). On 14 days after the first instillation, bronchial alveolar lavage (BAL) fluids were obtained from the lungs of all the live mice using media containing 2% FBS, and

pathological analysis of the lung tissues was performed following the standard operating procedure of the Korea Institute of Toxicology.

2.11. Statistical analysis

Mean values and standard deviations (SD) of data were calculated, and statistical significance of the treated groups with the control group was analyzed using one-way analysis of variance followed by post hoc Tukey's pairwise comparison (GraphPad Software, San Diego, CA, USA) and Student's *t*-test (SigmaPlot13, Systatsoftware Inc., Chicago, IL, USA). In addition, a *p*-value of less than 0.05 was considered to be significant.

3. Results

3.1. Characterization of DDAC in DW

Typical TEM images show that DDAC is in suspended state, but not soluble state, in DW and that diameters of suspended DDAC was around 55 nm for large particles and around 8 nm for small particles (Fig. 1). The surface charge of suspended DDAC was the neutral value (-0.89 mV). Meanwhile, contrary to our expectation, suspended DDAC was not detected in particle size analysis (data not show).

3.2. Decrease of cell viability following exposure to DDAC

In preliminary experiments, we found that the effect of DDAC on cell viability is dependent on the number of exposed cells (data not shown). When was seeded at density of 2×10^4 cells/mL (4000 cells/well) in a 96-well plate, cell viability sharply decreased at a 4 µg/mL of concentration, but it did not significantly increase at the higher concentration than 4 µg/mL (Fig. 2). Cell viability was 88.6 ± 7.5 , 82.1 ± 7.9 , 69.5 ± 12.2 , and $21.8 \pm 8.9\%$ compared with the control at a 0.5, 1, 2, and 4 µg/mL concentration, respectively.

3.3. Formation of a giant lamellar body-like structure

Under a phase contrast microscope, we found that the cell population notably decrease in DDAC (4 µg/mL)-treated group compared to that in the control group and that numerous vacuoles are formed in the

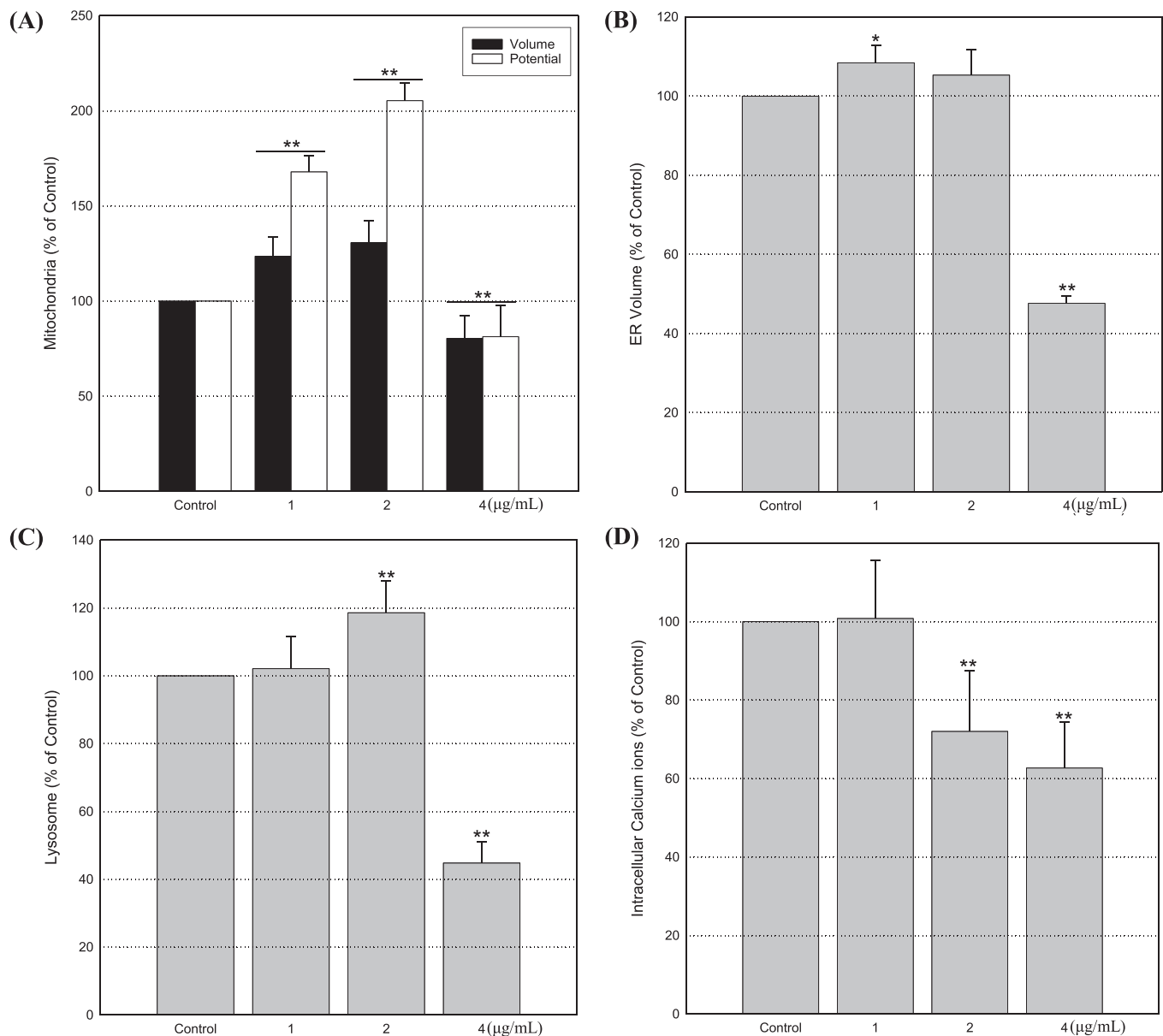


Fig. 6. Integrity of intracellular components.

Stabilized cells were incubated with or without DDAC for 24 h, the cells were then further incubated with the corresponding indicators according to the manufacturer's instructions. (A) Volume and potential of mitochondria, (B) ER volume, (C) lysosome volume and (D) mitochondrial Ca^{2+} . All data are presented as mean \pm SD of three independent experiments (N = 3).

cytosol of DDAC-treated cells (Fig. 3A). TEM images also revealed that vacuoles containing multi-membranes are formed in DDAC-treated cells (Supplementary Fig. 1), and that the structural features were very similar to the lamellar bodies (Weaver et al., 2002). In addition, the number of vacuoles tended to increase in cells exposed to 4 $\mu\text{g/mL}$ (Fig. 3C) compared to cells exposed to 2 $\mu\text{g/mL}$ (Fig. 3B). Furthermore, the mitochondria, nuclear components and pseudopodia seemed to disappear upon DDAC treatment, and organelles of different shapes were seen within the vacuoles.

3.4. Apoptotic cell death accompanying cell-membrane damage

Considering TEM images of DDAC (4 $\mu\text{g/mL}$)-treated cells, we measured the level of LDH released from the cells and Annexin V that

were bound to phosphatidyl serine exposed on the cell surface. Consistent with the effect on cell viability, the released LDH level increased rapidly at a concentration of 4 $\mu\text{g/mL}$, and the level was 83.6 ± 8.2 , 93.1 ± 11.9 , 102.7 ± 7.5 , and $169.4 \pm 21.7\%$ of the control at a 0.5, 1, 2, and 4 $\mu\text{g/mL}$ of dose, respectively (Fig. 4A). It was also $234.7 \pm 17.8\%$ of the control at a 8 $\mu\text{g/mL}$ (data not shown). Additionally, the proportion of cells in the late apoptotic cell death region was $9.6 \pm 3.8\%$ and $82.6 \pm 15.4\%$ in control and DDAC (4 $\mu\text{g/mL}$)-treated cells, respectively (Fig. 4B). Meanwhile, the cell death manner seemed to be modified into the necrotic (or necroptotic) cell death at the 8 $\mu\text{g/mL}$ dose, although there was no significant difference in cell viability (Fig. 1, Supplementary Fig. 2). While there was an apparent increase in intracellular complexity and a decrease in cell size (Supplementary Fig. 2, Park et al., 2018), no arrest in cell-cycle

Table 1
Up-regulated gene expression in DDAC-exposed cells.

| Gene_Symbol | mRNA Accession | 1st | 2nd | 3rd | AV | SD |
|--------------|-----------------|-------|-------|-------|-------|-------|
| CXCL8 | NM_000584 | 47.72 | 47.53 | 26.11 | 40.45 | 12.42 |
| IL24 | NM_001185156 | 52.03 | 30.22 | 9.33 | 30.53 | 21.35 |
| SLC7A11 | NM_014331 | 13.72 | 22.85 | 20.18 | 18.92 | 4.70 |
| MMP1 | NM_001145938 | 23.44 | 22.63 | 5.99 | 17.36 | 9.85 |
| IL1A | NM_000575 | 22.16 | 12.23 | 10.05 | 14.81 | 6.46 |
| | NONHSAT130229 | 13.72 | 11.11 | 12.64 | 12.49 | 1.31 |
| DDIT3 | NM_001195053 | 11.58 | 12.16 | 7.82 | 10.52 | 2.35 |
| TRIB3 | NM_001301188 | 7.86 | 13.89 | 8.23 | 9.99 | 3.38 |
| PTX3 | NM_002852 | 10.70 | 13.89 | 4.54 | 9.71 | 4.75 |
| HMOX1 | NM_002133 | 10.23 | 13.30 | 4.71 | 9.41 | 4.35 |
| DLGAP1-AS2 | NR_119377 | 11.27 | 7.48 | 9.37 | 9.37 | 1.89 |
| ASNS | NM_001178075 | 5.58 | 6.98 | 12.63 | 8.40 | 3.73 |
| TMEM156 | NM_001303228 | 9.30 | 7.74 | 5.74 | 7.59 | 1.78 |
| LOC541472 | NR_131935 | 8.82 | 7.93 | 5.11 | 7.29 | 1.94 |
| GDF15 | NM_004864 | 8.60 | 9.17 | 3.50 | 7.09 | 3.12 |
| ZFPM2-AS1 | NR_125796 | 7.70 | 6.33 | 5.81 | 6.61 | 0.97 |
| LURAP1L | NM_203403 | 7.82 | 5.87 | 5.29 | 6.33 | 1.32 |
| ALDH1L2 | NM_001034173 | 5.71 | 5.40 | 7.41 | 6.17 | 1.08 |
| DNAJB9 | NM_012328 | 7.04 | 7.34 | 3.80 | 6.06 | 1.96 |
| LURAP1L-AS1 | NR_125775 | 6.01 | 6.19 | 5.59 | 5.93 | 0.31 |
| IL6 | NM_000600 | 7.90 | 6.09 | 3.76 | 5.92 | 2.08 |
| MIR616 | NR_030346 | 7.06 | 5.58 | 5.10 | 5.91 | 1.02 |
| TNFAIP3 | NM_001270507 | 7.20 | 6.98 | 3.35 | 5.84 | 2.16 |
| | NONHSAT128246 | 7.33 | 3.71 | 6.43 | 5.82 | 1.88 |
| EREG | NM_001432 | 7.31 | 5.83 | 4.32 | 5.82 | 1.49 |
| NCR3LG1 | NM_001202439 | 6.24 | 5.21 | 5.77 | 5.74 | 0.52 |
| | NONHSAT115853 | 5.87 | 6.73 | 4.34 | 5.64 | 1.21 |
| PPP1R15A | NM_014330 | 6.82 | 5.43 | 3.62 | 5.29 | 1.60 |
| CREBRF | NM_001168393 | 4.00 | 6.55 | 5.03 | 5.19 | 1.28 |
| NCR3LG1 | XR_930865 | 6.40 | 4.93 | 4.03 | 5.12 | 1.20 |
| | NONHSAT002908 | 6.92 | 3.85 | 4.56 | 5.11 | 1.61 |
| HERPUD1 | NM_001010989 | 5.80 | 5.45 | 3.92 | 5.06 | 1.00 |
| ICAM1 | NM_000201 | 5.96 | 5.15 | 3.79 | 4.97 | 1.09 |
| SAT1 | NM_002970 | 7.14 | 4.81 | 2.94 | 4.96 | 2.10 |
| MOCOS | NM_017947 | 4.96 | 4.79 | 4.86 | 4.87 | 0.09 |
| ERN1 | NM_001433 | 5.01 | 6.21 | 3.33 | 4.85 | 1.45 |
| PSAT1 | NM_021154 | 3.52 | 4.25 | 6.62 | 4.80 | 1.62 |
| CEBPG | NM_001252296 | 4.26 | 5.95 | 3.91 | 4.71 | 1.09 |
| CLDN1 | NM_021101 | 5.24 | 4.82 | 4.07 | 4.71 | 0.59 |
| LOC344887 | NR_033752 | 7.04 | 4.33 | 2.56 | 4.64 | 2.26 |
| | ENST00000516454 | 1.31 | 13.67 | -1.14 | 4.61 | 7.94 |
| STC2 | NM_003714 | 3.54 | 5.51 | 4.79 | 4.61 | 0.99 |
| SESN2 | NM_031459 | 4.17 | 5.06 | 4.45 | 4.56 | 0.46 |
| KDM7A | NM_030647 | 3.30 | 5.89 | 4.11 | 4.43 | 1.32 |
| RPLP0P2 | NR_002775 | 5.42 | 4.83 | 2.97 | 4.40 | 1.28 |
| RNU11 | NR_004407 | 5.64 | 3.46 | 4.03 | 4.38 | 1.13 |
| SPG20-AS1 | NR_045180 | 4.78 | 2.70 | 5.34 | 4.28 | 1.39 |
| LOC105369502 | XR_913542 | 4.24 | 4.89 | 3.49 | 4.21 | 0.70 |
| SLC22A15 | NM_018420 | 3.61 | 5.02 | 3.71 | 4.11 | 0.78 |
| | ENST00000449457 | 5.27 | 3.37 | 3.49 | 4.04 | 1.07 |
| | NM_017644 | 4.83 | 1.90 | 5.29 | 4.01 | 1.84 |
| KLHL24 | NM_017644 | 2.95 | 4.00 | 4.91 | 3.95 | 0.98 |
| SMOX | NM_001270691 | 3.84 | 4.97 | 3.02 | 3.94 | 0.98 |
| SERPINB2 | NM_001143818 | 4.21 | 5.74 | 1.88 | 3.94 | 1.94 |
| YAE1D1 | NM_001282446 | 5.01 | 3.33 | 3.40 | 3.91 | 0.95 |
| ITGA2 | NM_002203 | 4.40 | 4.24 | 3.09 | 3.91 | 0.71 |
| | ENST00000440555 | 3.00 | 3.71 | 4.95 | 3.88 | 0.99 |
| MT1M | NM_176870 | 2.22 | 7.08 | 2.20 | 3.84 | 2.81 |

phases appeared to be involved in the DDAC-induced cell death (Fig. 4C). Based on the above observation, we determined to use 1, 2, and 4 $\mu\text{g}/\text{mL}$ concentrations for the subsequent experimentation.

3.5. Reduction of intracellular ROS

Numerous studies have focused on the role of free radicals (ROS and RNS) in the induction of cell death and inflammation (Adly, 2010; Auten and Davis, 2009). In this study, the generation of intracellular

Table 2
Down-regulated gene expression in DDAC-exposed cells.

| Gene_Symbol | mRNA Accession | 1st | 2nd | 3rd | AV | SD |
|--------------|-----------------|-------|-------|--------|-------|------|
| | ENST00000387314 | -4.01 | -7.19 | -11.75 | -7.65 | 3.89 |
| GJA1 | NM_000165 | -5.70 | -5.70 | -5.51 | -5.64 | 0.11 |
| | ENST00000384277 | -5.72 | -8.49 | -2.58 | -5.60 | 2.95 |
| | NONHSAT130345 | -3.51 | -7.59 | -4.85 | -5.32 | 2.08 |
| LOC105369559 | XR_913665 | -5.57 | -7.03 | -3.31 | -5.30 | 1.88 |
| MEST | NM_001253900 | -5.00 | -5.85 | -4.42 | -5.09 | 0.72 |
| MYL9 | NM_006097 | -3.97 | -6.00 | -4.61 | -4.86 | 1.03 |
| | ENST00000363156 | -2.47 | -6.84 | -4.89 | -4.73 | 2.19 |
| SKP2 | NM_001243120 | -5.12 | -5.82 | -3.15 | -4.70 | 1.38 |
| INHBB | NM_002193 | -4.58 | -4.14 | -5.33 | -4.69 | 0.60 |
| KIT | NM_000222 | -4.32 | -5.81 | -3.39 | -4.51 | 1.22 |
| PCDHB5 | NM_015669 | -6.39 | -4.19 | -2.82 | -4.47 | 1.80 |
| SLC38A4 | NM_001143824 | -4.63 | -5.95 | -2.75 | -4.44 | 1.61 |
| | NONHSAT130312 | -5.61 | -4.99 | -2.57 | -4.39 | 1.61 |
| ST6GALNAC5 | NM_030965 | -4.73 | -5.77 | -2.52 | -4.34 | 1.66 |
| | ENST00000441167 | -5.33 | -4.62 | -3.05 | -4.33 | 1.17 |
| CRISPLD2 | NM_031476 | -4.39 | -4.46 | -3.96 | -4.27 | 0.27 |
| PRR16 | NM_001300783 | -5.18 | -3.71 | -3.89 | -4.26 | 0.80 |
| LINC01111 | NR_105006 | -5.28 | -4.78 | -2.57 | -4.21 | 1.44 |
| RGS4 | NM_001102445 | -3.54 | -3.77 | -5.01 | -4.10 | 0.79 |
| GFRA1 | NM_001145453 | -4.71 | -4.09 | -3.45 | -4.08 | 0.63 |
| KIRREL3-AS2 | NR_046986 | -3.10 | -5.69 | -3.00 | -3.93 | 1.52 |
| LRRRC15 | NM_001135057 | -3.83 | -4.24 | -3.51 | -3.86 | 0.36 |
| CPA4 | NM_001163446 | -3.25 | -5.31 | -2.96 | -3.84 | 1.28 |
| MAP2K6 | NM_002758 | -4.47 | -3.19 | -3.85 | -3.84 | 0.64 |
| ATP2B4 | NM_001001396 | -4.06 | -3.41 | -3.86 | -3.77 | 0.33 |
| CCDC80 | NM_199511 | -4.10 | -4.57 | -2.64 | -3.77 | 1.01 |
| DKK1 | NM_012242 | -3.72 | -5.21 | -2.33 | -3.75 | 1.44 |
| | NONHSAT079576 | -2.58 | -5.30 | -3.32 | -3.73 | 1.41 |
| FHDC1 | NM_033393 | -4.55 | -4.14 | -2.46 | -3.72 | 1.11 |
| | NONHSAT047177 | -2.73 | -5.34 | -2.87 | -3.64 | 1.47 |
| LOC105376382 | XR_930613 | -2.97 | -6.31 | -1.52 | -3.60 | 2.46 |
| IFT1 | NM_001270927 | -4.91 | -4.05 | -1.69 | -3.55 | 1.67 |
| GAS6-AS2 | NR_044993 | -3.70 | -5.36 | -1.58 | -3.55 | 1.89 |
| COL1A1 | NM_000088 | -3.27 | -4.58 | -2.75 | -3.54 | 0.94 |
| COL8A1 | NM_001850 | -3.69 | -3.81 | -3.10 | -3.53 | 0.38 |
| CD24 | ENST00000610952 | -3.36 | -3.45 | -3.74 | -3.52 | 0.20 |
| IGFBP3 | NM_000598 | -2.68 | -3.86 | -4.00 | -3.52 | 0.73 |
| TMEM255A | NM_001104544 | -3.48 | -4.27 | -2.70 | -3.48 | 0.79 |
| ENC1 | NM_001256574 | -2.82 | -4.42 | -3.19 | -3.48 | 0.84 |
| THBS2 | NM_003247 | -3.84 | -3.33 | -3.20 | -3.46 | 0.34 |
| CCBE1 | NM_133459 | -3.46 | -3.75 | -3.16 | -3.45 | 0.30 |
| PDE1C | NM_001191056 | -3.94 | -3.68 | -2.72 | -3.44 | 0.64 |
| SERPINE1 | NM_000602 | -3.27 | -3.53 | -3.44 | -3.41 | 0.13 |
| TMEM14A | NM_014051 | -3.26 | -4.23 | -2.56 | -3.35 | 0.84 |
| LOC648570 | AK130915 | -3.92 | -3.92 | -2.15 | -3.33 | 1.02 |
| | ENST00000558905 | -1.88 | -4.74 | -3.35 | -3.32 | 1.43 |
| MATN2 | NM_002380 | -4.06 | -3.58 | -2.28 | -3.31 | 0.92 |
| NREP | NM_001142474 | -3.81 | -3.46 | -2.64 | -3.30 | 0.60 |
| MIR3167 | NR_036126 | -2.53 | -4.19 | -3.18 | -3.30 | 0.84 |
| | ENST00000515947 | -3.92 | -3.38 | -2.59 | -3.30 | 0.67 |
| | NONHSAT118989 | -2.28 | -5.86 | -1.67 | -3.27 | 2.26 |
| NPR3 | NM_000908 | -3.39 | -4.79 | -1.62 | -3.27 | 1.59 |
| | NONHSAT123337 | -3.48 | -3.32 | -2.99 | -3.27 | 0.25 |
| FLNC | NM_001127487 | -2.60 | -3.31 | -3.84 | -3.25 | 0.62 |
| TAGLN | NM_001001522 | -3.59 | -3.11 | -3.01 | -3.24 | 0.31 |
| | ENST00000387456 | -1.85 | -3.67 | -4.10 | -3.21 | 1.19 |

ROS was rapidly inhibited in cells treated at a 4 $\mu\text{g}/\text{mL}$ concentration ($48.8 \pm 12.0\%$ compared to control), whereas there was no significant change in the NO level at the same concentration ($93.7 \pm 3.9\%$ of the control) (Fig. 5).

3.6. Structural damage of intracellular organelles

The mitochondrial volume and potential were significantly elevated in cells exposed to 1 $\mu\text{g}/\text{mL}$ ($123.6 \pm 10.2\%$ and $167.9 \pm 8.6\%$ of the

control, respectively) and 2 $\mu\text{g}/\text{mL}$ ($130.7 \pm 11.6\%$ and $205.3 \pm 9.3\%$ of the control, respectively) of DDAC (Fig. 6A), whereas the volume of ER ($108.4 \pm 4.4\%$ and $105.3 \pm 6.5\%$ of the control, Fig. 6B) and lysosomes ($102.1 \pm 9.5\%$ and $118.6 \pm 9.3\%$ of the control, Fig. 6C) did not notably change at the same concentrations. Meanwhile, when treated at 4 $\mu\text{g}/\text{mL}$ of concentration, the volume of the mitochondria ($80.4 \pm 11.8\%$), ER ($47.6 \pm 2.0\%$), and lysosome ($44.8 \pm 6.3\%$) were clearly reduced compared to the control, mitochondrial calcium levels (Fig. 6D) also decreased to $81.2 \pm 16.3\%$ and $62.7 \pm 11.7\%$ of the control at the same concentration, respectively.

3.7. Gene profile changes

The average total number of genes up-regulated more than two folds was 616 ± 66.9 , and that of genes down-regulated less than two folds was 473 ± 171.0 . As shown in Tables 1 and 2, expression of immune response-related genes including CXCL8, IL-24 and IL-1A, the most increased, whereas that of gap junction alpha-1 (GJA1) which is a component of gap junctions, and mesoderm-specific transcript (MEST) which is a maternally imprinted gene that is involved in carcinogenesis (Li et al., 2015) was the most down-regulated. KEGG pathway analysis also suggested that metabolic and TNF signaling pathway are the most involved in DDAC-induced gene expression (Supplementary Fig. 3).

3.8. Effects on protein expression

Expression of surfactant proteins (SP-A, -B, and -D), ABCA3 and Rab11a, (lamellar body formation, Cheong et al., 2007), p-p53 (damaged DNA repair), CLIC4 (primarily localized in the outer mitochondrial membrane, Gururaja Rao et al., 2020), Apaf-1 (apoptosome formation), DRP-1 (mitochondrial fission), MFN1 (mitochondrial fusion), and p62 (autophagosome cargo protein) was enhanced in DDAC-treated cells compared to that in the control, and caspase-3 protein was rapidly cleaved at a concentration of 4 $\mu\text{g}/\text{mL}$ (Fig. 7). The levels of V-ATPase (a proton pump for cellular pH regulation, Pamarthy et al., 2018), LAMP-2 (a lysosome-associated membrane glycoprotein), PARP (genomic stability), fibrillarin (a small nucleolar protein, Amin et al., 2007), and EGFR (a transmembrane protein) were clearly reduced at the same concentration. Additionally, conversion of LC3B-I into LC3B-II (completion of autophagosome) and expression of OPA1 (localized in the inner mitochondrial membrane) and CLIC1 (principally localized in the cell nucleus, Gururaja Rao et al., 2020) proteins did not show significant changes following exposure to DDAC. Secretion of proinflammatory cytokines (IL-1 β , IL-6, and TNF- α) and MMP-1 (known as interstitial collagenase) was significantly elevated with DDAC concentration, whereas secretion of IFN- γ , MIP-1 α , CXCL-1, CXCL-8, and MMP-3 was not affected under the same conditions (Fig. 8).

3.9. Lamellar bodies formed in the lungs of DDAC-treated mice

When a single instilled with 2000, 1000, 500, 250, and 125 μg of DDAC (32.5 ± 1.9 g, three mice per concentration) to predict the acute toxicity level, all mice treated at a 2000 and 1000 μg died within 24 h after a single instillation, whereas all the mice exposed to doses less than 500 μg were alive at 14 days. We then instilled DDAC twice (weekly, 12 mice/sex/dose, 500, 250 and 125 μg) for 14 days to identify a cause of the sudden death. While dosing-related body weight changes were not observed in both sexes of mice (Supplementary Fig. 4), each nine mice died in male and female groups exposed to the maximum dose on day 3 or 4 after the second instillation. We also found chronic fibrotic pulmonary lesion (Fig. 8, A and B) and thymus atrophy (Fig. 8C) in three mice that survived in the highest-dosed group (Table 3). Additionally, TEM images revealed that numerous lamellar bodies are formed in the lungs of mice exposed to DDAC (Fig. 9). Meanwhile, contrary to our expectation (Anderson et al., 2016), the level of IL-4 and IFN- γ showed

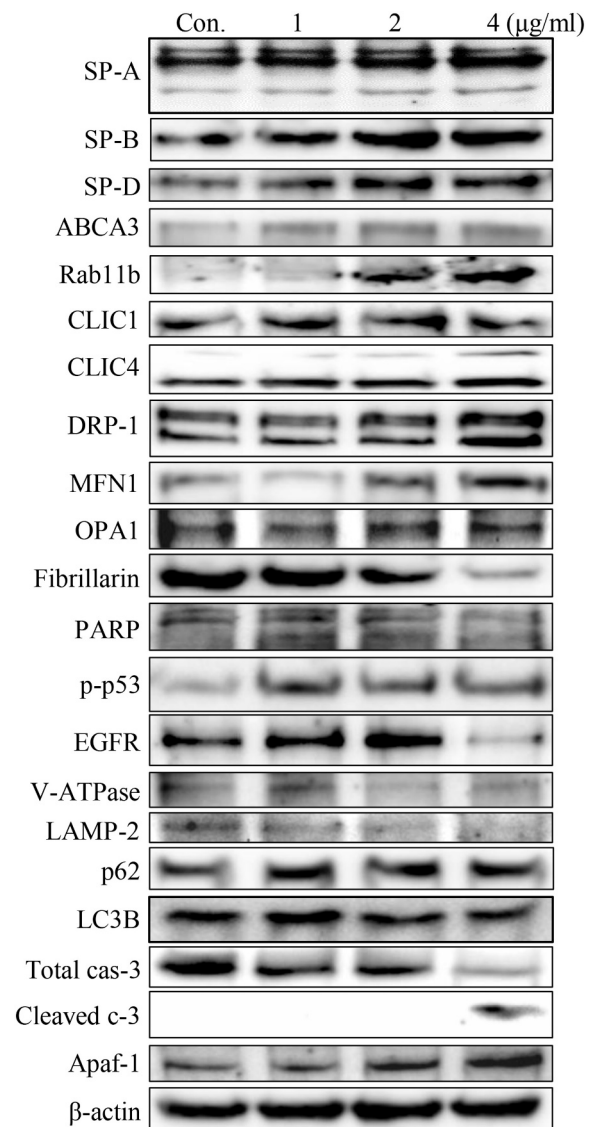


Fig. 7. Changes in protein expression.

Cells were harvested at 24 h after exposure to DDAC, and blotting of each protein was done independently three times. The expression of all proteins showed the same trends, and representative images were loaded.

the decreasing trend in the lung of both sexes of mice treated with DDAC compared to control, and the levels of most of cytokines (or chemokines) were not significantly different between groups (Supplementary Fig. 5).

4. Discussion

Although the mechanism of its action is unclear, it is currently known that corona virus may remain viable for hours to days in the environment. The U.S. CDC recommends cleaning and disinfecting household products along with improvement of the ventilation systems to limit the spread of infection by indirect exposure (U.S. CDC, 2020), thus a large amount of disinfectant ingredients are releasing into the environment. Almost all cell membranes of microorganisms including viruses, and many of their intracellular organelles including the nucleus, ER, Golgi apparatus, lysosome, and mitochondria are surrounded by one or two membranes that consist of lipid bilayers, amphiphilic phospholipids are the major components. Therefore, detergent ingredients have often been applied in antimicrobial agents such as disinfectants and antiseptics as well as in daily consumer products such as fabric softeners, various types of cleaners, air

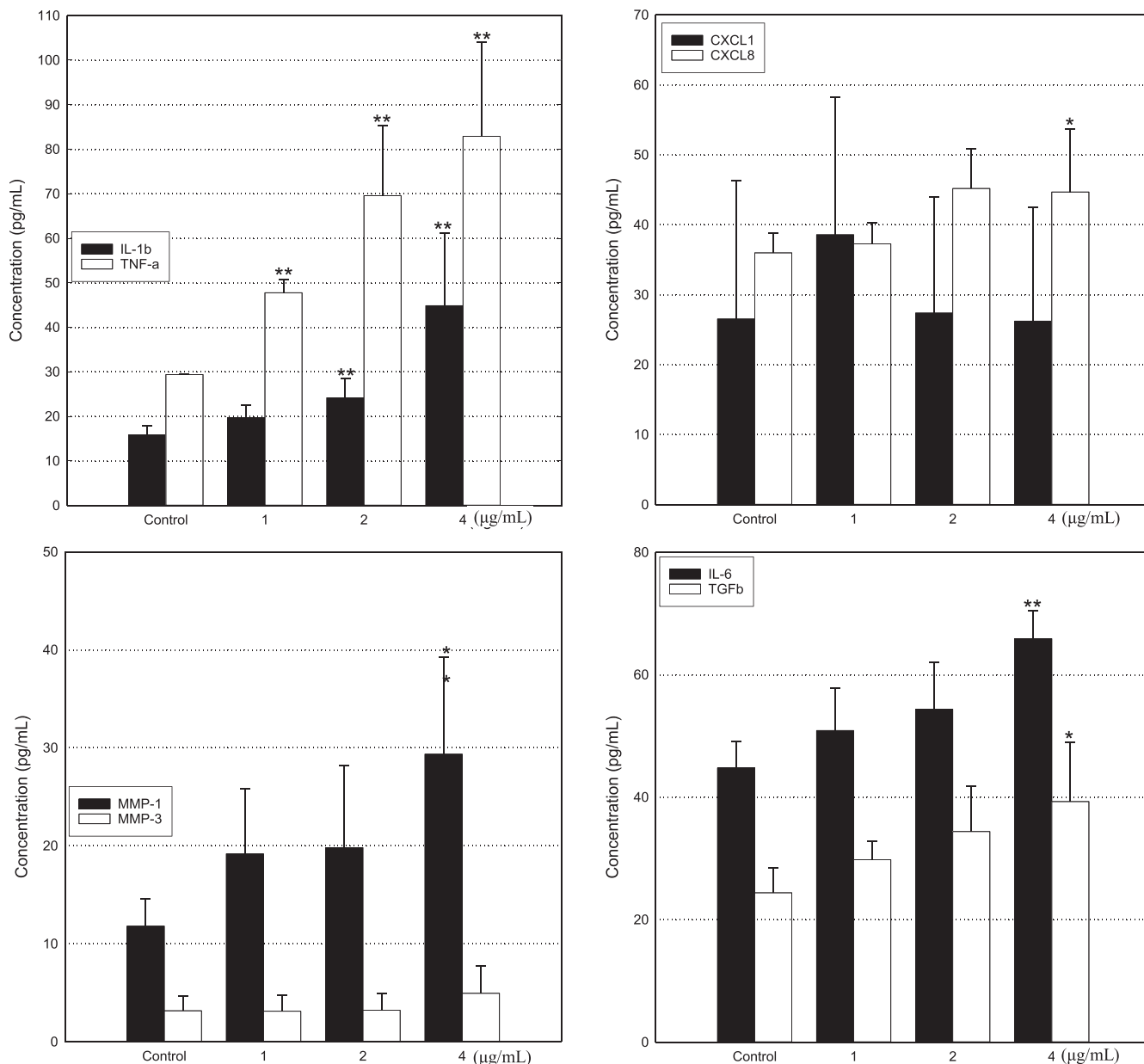


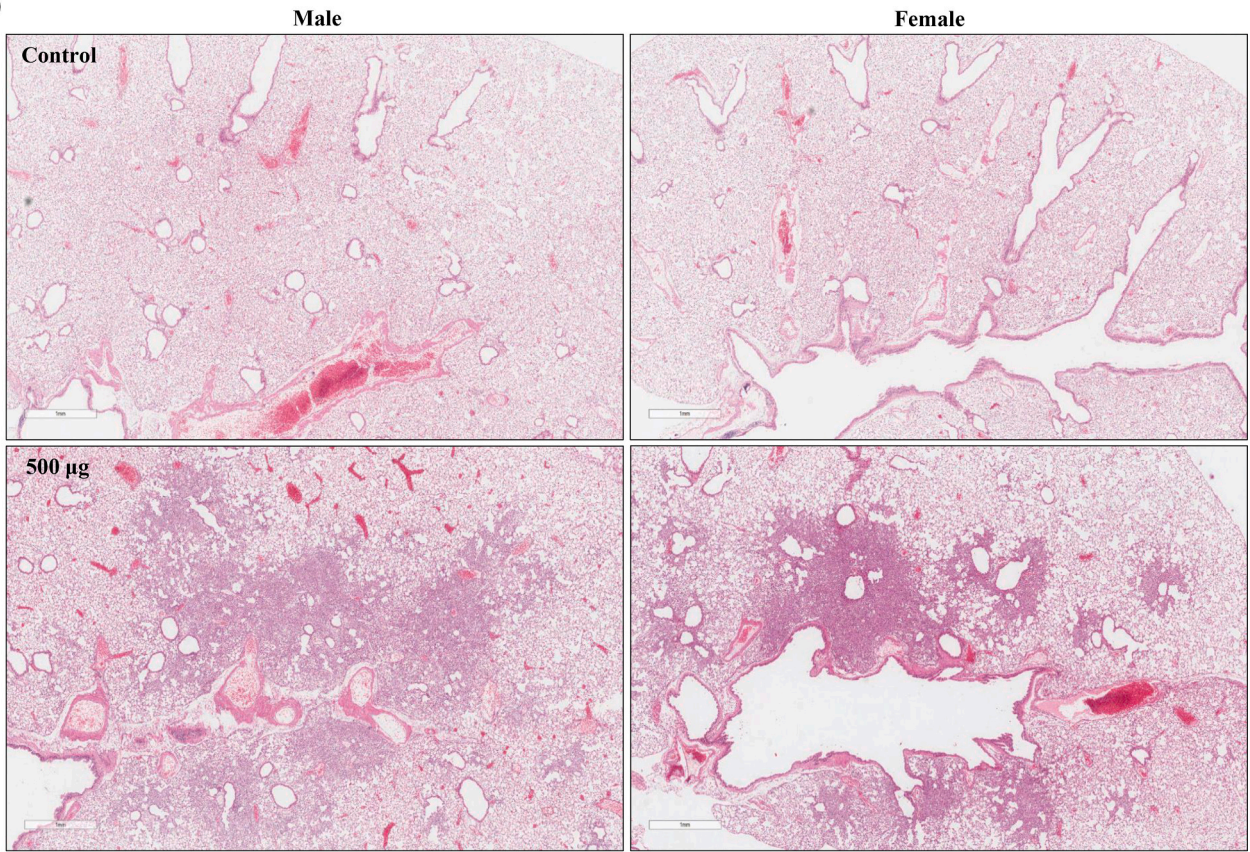
Fig. 8. Secretion of soluble proteins.

Considering that DDAC induced cell death was started at early time (about 3–6 h after exposure), we evaluated effects on secretion of cell communication-related proteins on 6 h after DDAC treatment. All experiments were performed independently four times using 2 wells per sample, and the level of each protein was calculated using a standard curve produced under the same conditions.

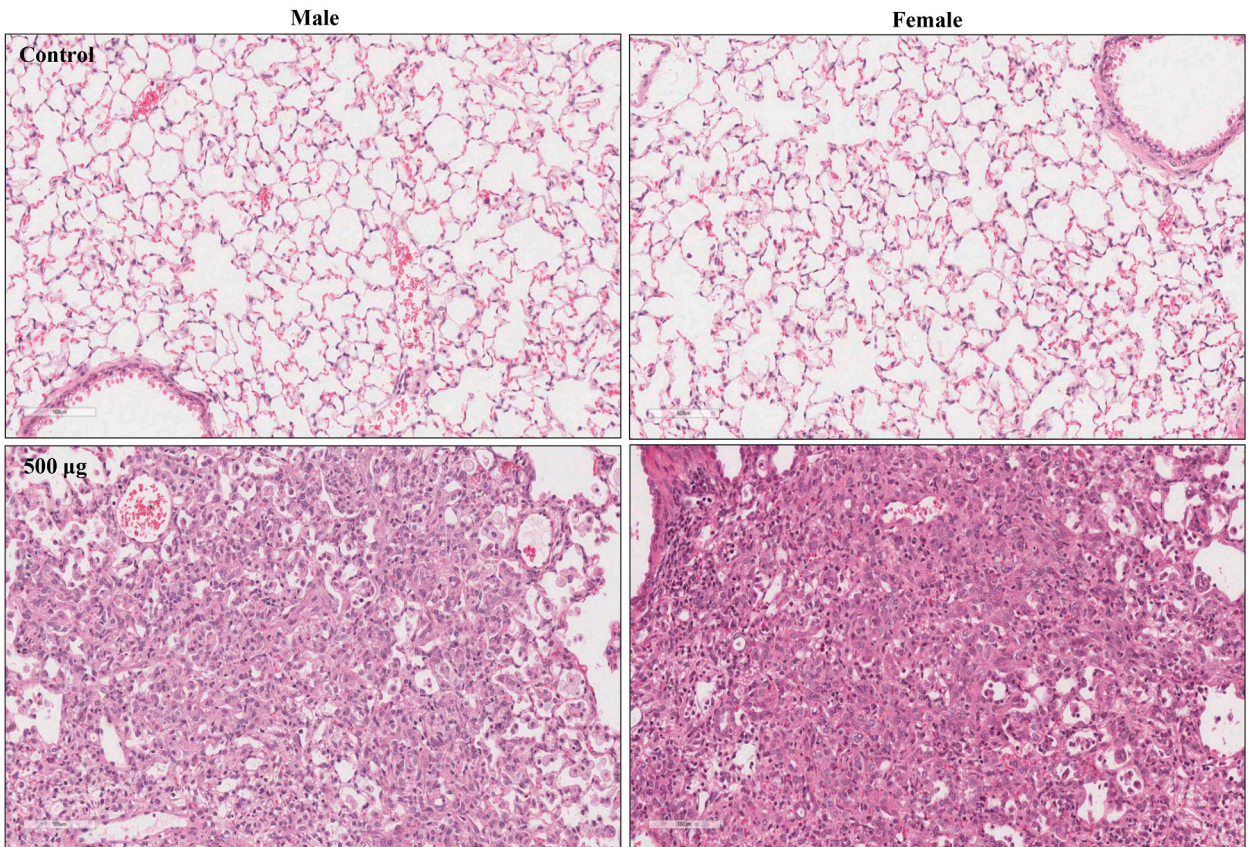
fresheners and deodorants (Schuck et al., 2003). Disinfectants are non-selective agents that kill a wide range of microbes on non-living surfaces to prevent the spread of illness, and antiseptics are applied to living tissues to reduce the possibility of infection, especially during surgery. EPA registered DDAC as a pesticide and anticipated that exposure by inhalation or ingestion as well as through the skin or eyes might be possible. As previously stated, DDAC has been also widely used for commercial and residential applications as an antimicrobial, and its solutions are added to humidifiers, fabric refreshers, cooling systems, and water-storage tanks (Pubchem, 2005). Furthermore, DDAC was one of the ingredients in humidifier disinfectants that caused idiopathic lung diseases in Korea since 2006. In our previous studies using humidifier disinfectant ingredients

such as PHMG-phosphate, MIT, and Kathon, we emphasized the impact of the critical micelle concentration (CMC) on cell death induced by detergents that have amphiphilic activity (Park et al., 2018; Park et al., 2020; Park and Seong, 2020). In this study, we again demonstrated that cell viability dramatically decrease at a concentration of 4 µg/mL and that there was no significant change in cell viability at higher concentrations. In addition, the cytotoxic level was closely associated with the number of exposed cells. The CMC is the concentration at which surfactants start forming micelles, and the European Union (2015) reported that the CMC of DDAC is 650 µg/mL at 20 ± 0.5 °C. Experimental conditions including pH, buffer composition, and temperature are key factors determining the CMC of detergents (Kang et al., 2001; Meta et al., 2005; Xu et al., 2009),

(A)



(B)



(caption on next page)

Fig. 9. Acute toxic response following DDAC instillation to mice.

DDAC (0, 125, 250, or 500 µg, male and female, 12 mice/sex/dose, weekly) was instilled into the lungs of mice via the trachea. On day 14 after instillation, all mice in the control, 125, and 250 µg groups were alive, whereas only three male and female mice were alive in the 500 µg-instilled group. Low (A) and high (B)-magnification for chronic interstitial inflammation with fibrosis. (C) Thymus atrophy. (D) TEM image of the lungs from DDAC (250 µg)-instilled mice.

and BEAS-2B cells were incubated with DDAC in culture media containing 10% FBS at 37 °C in a 5% CO₂ incubator. Given that DDAC is one of the QACs that can bind strongly to negative charges on cell membranes and that the surface charge and morphology were rapidly altered in phosphate buffered saline (PBS), an isotonic solution which match the osmolarity and ion concentrations (Supplementary Fig. 6), we hypothesize that DDAC could induce cytotoxicity at concentrations lower than the known CMC (650 µg/mL), and that it may be due to charge effects.

The membranes surrounding intracellular organelles permit the organelles to maintain the specific environment by dividing the contents within a single cell, thus maintaining normal cell function (Casares et al., 2019). Numerous researchers also suggested that excessive generation of free radicals may be a trigger that initiates the death signal, and that these radicals can impair the function of both the intracellular organelles and the plasma membrane. When treated with DDAC at a 4 µg/mL concentration, the LDH released out of the cells increased significantly compared with control, indicating the cell membrane damage, and the volume and potential of the mitochondria and the concentration of calcium ion in them clearly decreased accompanied by reduction in volume of ER and lysosome. Damage of the nuclear envelope and loss of nuclear contents were also observed in TEM images, and the expression of fibrillarlin, a C/D class small nucleolar ribonucleoprotein (Reichow et al., 2007), was rapidly inhibited following DDAC exposure. Similarly, gene-profile analysis using microarray techniques showed that DDAC enhances the expression of DNA damage-related genes such as DNA-damage-inducible transcript 3 (DDIT3, Lin et al., 2020), DLGAP1 antisense RNA 2 (DLGAP1-AS2), and microRNA616. Lamellar bodies were notably formed in the cytosol of DDAC-treated cells accompanying the enhanced expression of ABCA3 and Rab11a protein, known as the indicator (Yamano et al., 2001; Reynier et al., 2016), and amounts of the bodies remarkably seemed to increase in cells exposed to 4 µg/mL compared to 2 µg/mL of DDAC. Additionally, the intracellular ROS level rapidly decreased at a 4 µg/mL concentration, whereas the produced NO level did not show significant change up to 4 µg/mL. Furthermore, mitochondria seemed to disappear in DDAC-treated cells. The membrane of organelles such as the mitochondria, lysosome, and ER are also negatively charged, and electron-transfer processing by mitochondria is a central source in generation of intracellular ROS (Lim, 2004). Meanwhile, RNS is produced by the metabolism of amino acids and regulated by the intracellular Ca²⁺ level (Di Meo et al., 2016). Therefore, we suggest that the formation of lamellar bodies may trigger DDAC-induced cell death. Considering that DDAC can form layers in biofriendly solutions such as DW, PBS, cell culture media, and artificial lung lavage, we also hypothesize that exposure to DDAC may result in a loss of the contents by binding to the membranes of organelles as well as the cell membranes, and that DDAC itself or its conjugates with the cellular-system components may partially contribute to the lamellar body formation.

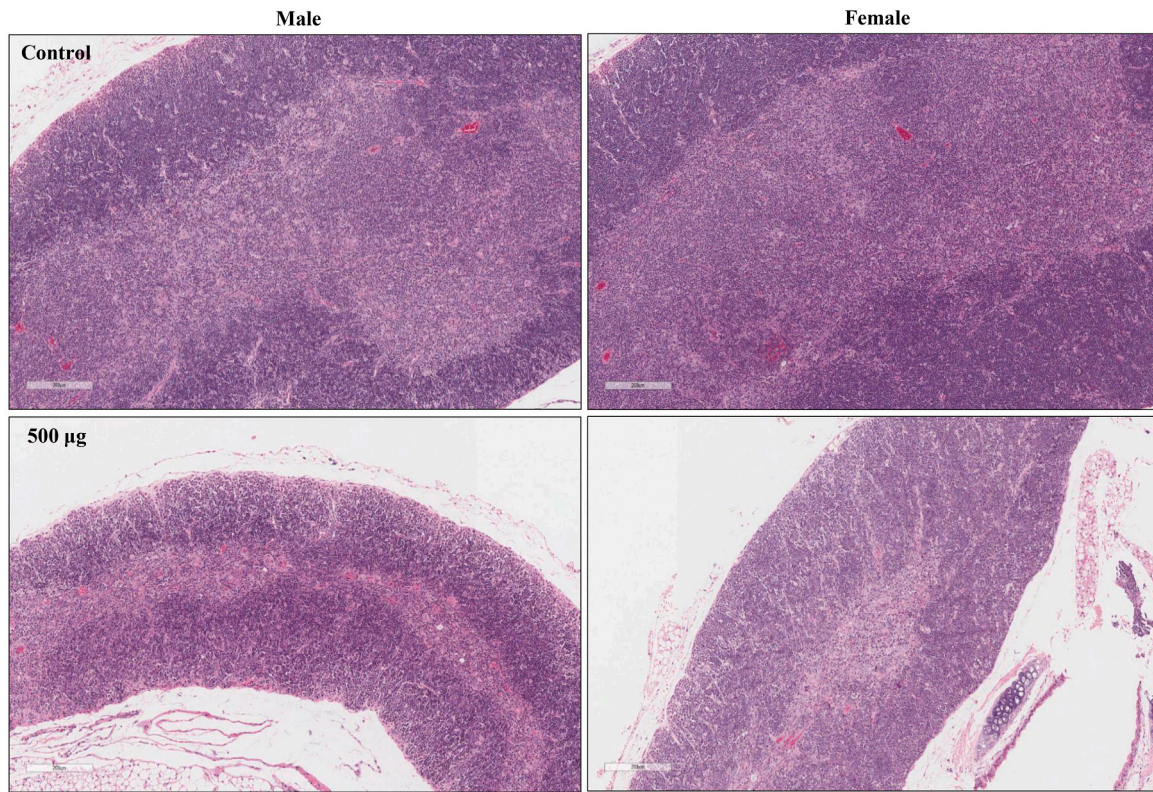
Accumulated evidence demonstrates that the balance between cell death and cell survival should be tightly controlled for tissue homeostasis and disease prevention and thus disruption of the balance can result in the development and progression of diseases, especially cancer (Gudipaty et al., 2018; Gong et al., 2019; Fond and Ravichandran, 2016). Additionally, different forms of cell death can be initiated by death signals that are triggered by intrinsic and extrinsic environments. The cell death forms can also be altered under intracellular conditions, and the properties of the debris can influence the type of biological immune response

that develops. As a representative example, apoptotic bodies can be removed from the body without causing inflammation by sending 'eat me' signal to the surrounding immune cells (Fogarty and Bergmann, 2015), whereas necrotic cell debris activates an inflammatory response (Rock and Kono, 2008; Westman et al., 2020). In this study, DDAC (4 µg/mL) formed apoptotic bodies without inducing specific cell-cycle arrests, whereas secretion of MMP-1 and proinflammatory cytokines (IL-1β, IL-6, and TNF-α) was clearly enhanced following DDAC exposure. The expression of genes that contribute to the activation of MMP-1 (IL-24, IL-1α, and pentraxin 3) was also remarkably elevated in DDAC-treated cells compared to that in control cells (Guo et al., 2012; Jin et al., 2014; Wang et al., 2005). In addition, nine of the twelve mice that were instilled twice (once in a week) to 500 µg of DDAC died on day 3 (or day 4) after the second instillation, and chronic fibrotic lesions were remarkably observed in male and female mice. Meanwhile, the pulmonary levels of inflammatory cytokines (or chemokines) was not distinctly altered in mice instilled with lower doses (125 and 250 µg) of DDAC. Herein, we hypothesize that the explosive increase in DDAC-induced apoptotic cell debris is responsible for the development of pulmonary fibrosis (Leverrier et al., 2001; Rovere-Querini et al., 2008; Park et al., 2018).

EPA classified DDAC as a chemical that is not likely to be carcinogenic to humans (U.S. EPA, 2005). However, some researchers have demonstrated that the formation of giant lamellar bodies is associated with pulmonary lymphoma of mucosa-associated lymphoid tissue origin, interstitial pneumonia, and adenocarcinoma of the lung. In our study, lamellar body-like structures were frequently observed both in the lung tissues from DDAC-instilled mice and BEAS-2B cells. Furthermore, pulmonary fibrotic lesions were developed together with atrophy of the thymus in DDAC-instilled mice. Lamellar bodies are specific structures for the storage of surfactant phospholipids which are tightly packed. Newly synthesized surfactant proteins are transported from organelles such as Golgi or ER to lamellar bodies via various pathways, and the reorganization of the intravesicular lipid structure is partially regulated by SP-B (Lu et al., 2018). Additionally, pulmonary surfactants regulate defense mechanisms and reduce surface tension (Shane et al., 2019; Uhliarova et al., 2016). For example, patients with Niemann-Pick type C2, a type of lysosomal-storage disorder, often present with adulthood interstitial lung disease and respiratory distress. In this disease, NPC2 gene mutations hinder the binding of unesterified cholesterol and the transportation of cholesterol to phospholipid vesicles, resulting in the change of composition of surfactant and the accumulation of enlarged lamellar bodies that are involved in inflammation and fibrosis of the lung parenchyma (Cheruku et al., 2006; Roszell et al., 2012). Similarly, in case of familial idiopathic pulmonary fibrosis (IPF), accumulation of mutant pulmonary SP-C causes ER stress and endothelial dysfunction via increased endothelin-1, decreased NO, and endothelial cell apoptosis that augment lung fibrosis (Naiel et al., 2019; Garcia, 2018). Furthermore, a human BAL fluid analysis showed that surfactant dysfunctions are typical features of IPF (Günther et al., 1999). Considering that intratracheal instillation technique, which does not mimic realistic human inhalation exposure and can result in severe local inflammatory response, was used for DDAC exposure in this study, we suggest that further study on the potential adverse health effects resulting from chronic inhalation of DDAC is needed to maintain the pulmonary health of the public (Ohnuma et al., 2010).

Supplementary data to this article can be found online at <https://doi.org/10.1016/j.taap.2020.115182>.

(C)



(D)

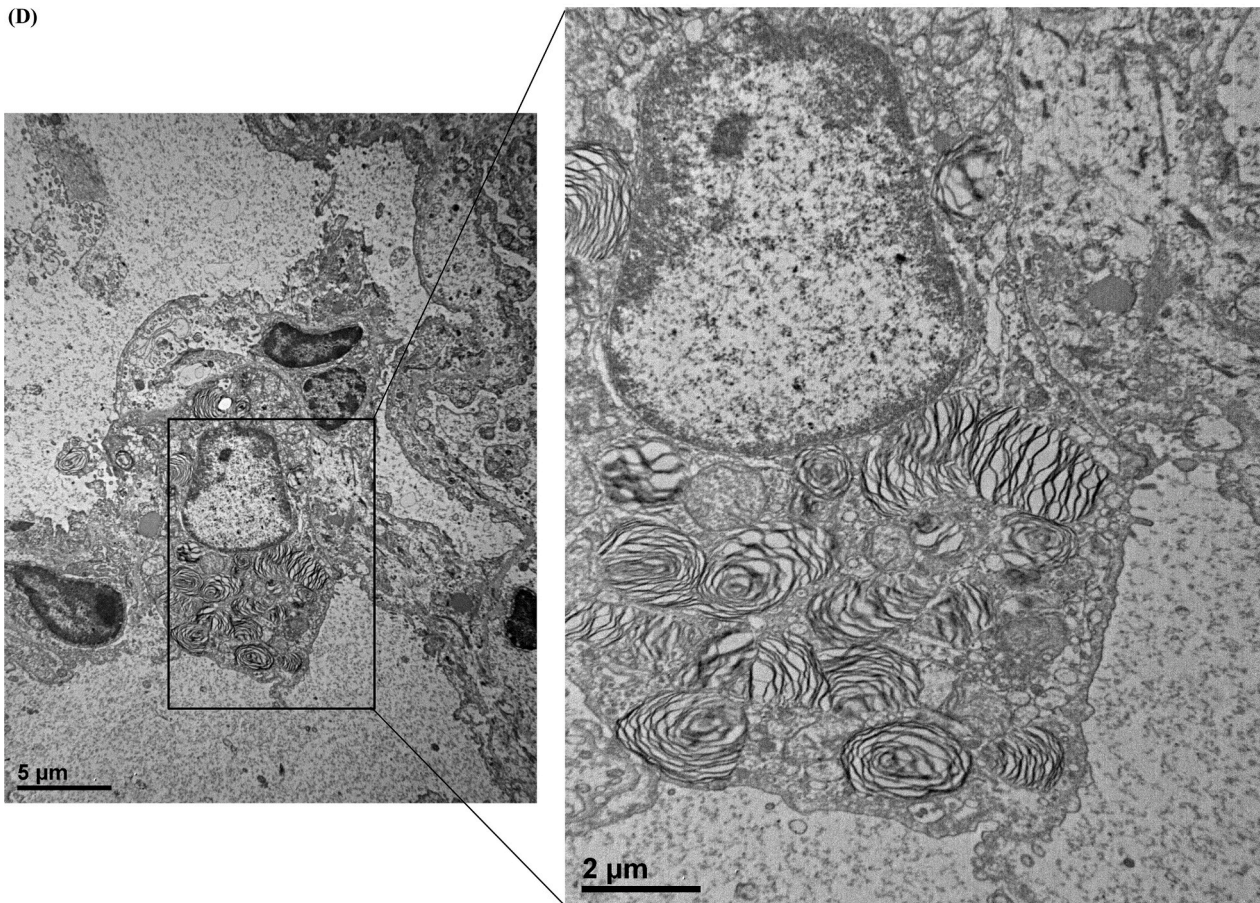


Fig. 9. (continued)

Table 3
Summary of the treatment-related microscopic findings.

| Tissues | Lesion | Male | | | | | | Female | | | | | | | |
|---------|------------------------------------|---------|---|---|---|--------|---|---------|---|---|---|--------|---|---|---|
| | | Control | | | | 500 µg | | Control | | | | 500 µg | | | |
| | | 1 | 2 | 3 | 4 | 1 | 2 | 3 | 4 | 1 | 2 | 3 | | | |
| Lung | Inflammation, chronic interstitial | - | - | - | - | - | 3 | 4 | - | - | - | - | 3 | 4 | 3 |
| | Fibrosis | - | - | - | - | - | 2 | 2 | - | - | - | - | 2 | 3 | 2 |
| | Aggregate, alveolar macrophage | - | - | - | - | 2 | - | - | - | - | - | - | - | - | - |
| Spleen | Extramedullary hemopoiesis | - | - | - | 1 | 1 | - | 1 | - | - | - | - | - | 2 | - |
| | Decreased size, follicle | - | - | - | - | - | - | - | - | - | - | - | 1 | - | - |
| Thymus | Epithelial cyst/tubules | - | - | - | - | 1 | - | - | - | - | - | - | - | - | - |
| | Atrophy | - | - | - | - | 1 | 1 | - | - | - | - | - | 1 | 1 | - |

*-; No remarkable change, '1'; Minimal, '2'; Slight, '3'; Moderate, '4'; Marked, '5'; Severe.

Declaration of Competing Interest

The authors declare that there are no conflicts of interest.

Acknowledgement

This work was supported by a grant from Kyung Hee University in 2018 (20180872 and 20182222) and the Ministry of Science and ICT (NRF-2015M3A7B6027948 and NRF-2016M3A9C4953144).

References

Adly, A.A.M., 2010. Oxidative stress and disease: an updated review. *Res. J. Immunol.* 3, 129–145.

Amin, M.A., Matsunaga, S., Ma, N., Takata, H., Yokoyama, M., Uchiyama, S., Fukui, K., 2007. Fibrillarin, a nucleolar protein, is required for normal nuclear morphology and cellular growth in HeLa cells. *Biochem. Biophys. Res. Commun.* 360, 320–326.

Anderson, S.E., Shane, H., Long, C., Lukomska, E., Meade, B.J., Marshall, N.B., 2016. Evaluation of the irritancy and hypersensitivity potential following topical application of didecylmethylammonium chloride. *J. Immunotoxicol.* 13, 557–566.

Auten, R.L., Davis, J.M., 2009. Oxygen toxicity and reactive oxygen species: the devil is in the details. *Pediatr. Res.* 66, 121–127.

Casares, D., Escribá, P.V., Rosselló, C.A., 2019. Membrane lipid composition: effect on membrane organelle structure, function and compartmentalization and therapeutic avenues. *Int. J. Mol. Sci.* 20 (pii:E2167).

CDC, 2020. Cleaning and Disinfection for Households. <https://www.cdc.gov/coronavirus/2019-ncov/prevent-getting-sick/cleaning-disinfection.html> (accessed 18 May 2020).

Cheong, N., Zhang, H., Madesh, M., Zhao, M., Yu, K., Dodia, C., Fisher, A.B., Savani, R.C., Shuman, H., 2007. ABCA3 is critical for lamellar body biogenesis in vivo. *J. Biol. Chem.* 282, 23811–23817.

Cheruku, S.R., Xu, Z., Dutia, R., Lobel, P., Storch, J., 2006. Mechanism of cholesterol transfer from the Niemann-Pick type C2 protein to model membranes supports a role in lysosomal cholesterol transport. *J. Biol. Chem.* 281, 31594–31604.

Consumer Product Information Database, 2020. Didecyl Dimethyl Ammonium Chloride. <https://www.whatsinproducts.com/chemicals/view/1/1297/007173-51-5/Didecyl%20dimethyl%20ammonium%20chloride/> (accessed 18 May 2020).

Di Meo, S., Reed, T.T., Venditti, P., Victor, V.M., 2016. Role of ROS and RNS sources in physiological and pathological conditions. *Oxidative Med. Cell. Longev.* 2016, 1245049.

European Union, 2015. Directive 98/8/EC Concerning the Placing Biocidal Products on the Market. Inclusion of Active Substances in Annex I to Directive 98/8/EC. Assessment Report. Didecylmethylammonium Chloride Product-type 8 (Wood Preservative). http://dissemination.echa.europa.eu/Biocides/ActiveSubstances/0067-08/0067-08_Assessment_Report.pdf (accessed 18 May 2020).

Fogarty, C.E., Bergmann, A., 2015. The sound of silence: signaling by apoptotic cells. *Curr. Top. Dev. Biol.* 114, 241–265.

Fond, A.M., Ravichandran, K.S., 2016. Clearance of dying cells by phagocytes: mechanisms and implications for disease pathogenesis. *Adv. Exp. Med. Biol.* 930, 25–49.

Garcia, C.K., 2018. Insights from human genetic studies of lung and organ fibrosis. *J. Clin. Invest.* 128, 36–44.

Gerba, C.P., 2015. Quaternary ammonium biocides: efficacy in application. *Appl. Environ. Microbiol.* 81, 464–469.

Gilbert, P., Moore, L.E., 2005. Cationic antiseptics: diversity of action under a common epithet. *J. Appl. Microbiol.* 99, 703–715.

Gong, Y.N., Crawford, J.C., Heckmann, B.L., Green, D.R., 2019. To the edge of cell death and back. *FEBS J.* 286, 430–440.

Gudipaty, S.A., Conner, C.M., Rosenblatt, J., Montell, D.J., 2018. Unconventional ways to live and die: cell death and survival in development, homeostasis, and disease. *Annu. Rev. Cell Dev. Biol.* 34, 311–332.

Günther, A., Schmidt, R., Nix, F., Yabut-Perez, M., Guth, C., Rosseau, S., Siebert, C., Grimming, F., Morr, H., Velcovsky, H.G., Seeger, W., 1999. Surfactant

abnormalities in idiopathic pulmonary fibrosis, hypersensitivity pneumonitis and sarcoidosis. *Eur. Respir. J.* 14, 565–573.

Guo, P., Zhang, S.Z., He, H., Zhu, Y.T., Tseng, S.C., 2012. PTX3 controls activation of matrix metalloproteinase 1 and apoptosis in conjunctivochalasis fibroblasts. *Invest. Ophthalmol. Vis. Sci.* 53, 3413–3423.

Gururaja Rao, S., Patel, N.J., Singh, H., 2020. Intracellular chloride channels: novel biomarkers in diseases. *Front. Physiol.* 11, 96.

Hegstad, K., Langsrud, S., Lunestad, B.T., Scheie, A.A., Sunde, M., Yazdankhah, S.P., 2010. Does the wide use of quaternary ammonium compounds enhance the selection and spread of antimicrobial resistance and thus threaten our health? *Microb. Drug Resist.* 16, 91–104.

Hrubec, T.C., Melin, V.E., Shea, C.S., Ferguson, E.E., Garofola, C., Repine, C.M., Chapman, T.W., Patel, H.R., Razvi, R.M., Sugrue, J.E., Potineni, H., Magnin-Bissel, G., Hunt, P.A., 2017. Ambient and dosed exposure to quaternary ammonium disinfectants causes neural tube defects in rodents. *Birth Defects Res.* 109, 1166–1178.

Jansen, A.C., Boucher, C.E., Coetsee, E., Kock, J.L.F., Van Wyk, P.W.J., Swart, H.C., Bragg, R.R., 2013. The influence of didecylmethylammonium chloride on the morphology and elemental composition of *Staphylococcus aureus* as determined by NanoSAM. *Sci. Res. Essays* 8, 152–160.

Jin, S.H., Choi, D., Chun, Y.J., Noh, M., 2014. Keratinocyte-derived IL-24 plays a role in the positive feedback regulation of epidermal inflammation in response to environmental and endogenous toxic stressors. *Toxicol. Appl. Pharmacol.* 280, 199–206.

Kang, K.H., Kin, H.U., Lim, K.H., 2001. Effect of temperature on critical micelle concentration and thermodynamic potentials of micellization of anionic ammonium dodecyl sulfate and cationic octadecyl trimethyl ammonium chloride. *Colloids Surf. A Physicochem. Eng. Asp.* 189, 113–121.

Kim, K.W., Ahn, K., Yang, H.J., Lee, S., Park, J.D., Kim, W.K., Kim, J.T., Kim, H.H., Rha, Y.H., Park, Y.M., Sohn, M.H., Oh, J.W., Lee, H.R., Lim, D.H., Choung, J.T., Han, M.Y., Lee, E., Kim, H.Y., Seo, J.H., Kim, B.J., Cho, Y.A., Do, K.H., Kim, S.A., Jang, S.J., Lee, M.S., Kim, H.J., Kwon, G.Y., Park, J.H., Gwack, J., Youn, S.K., Kwon, J.W., Jun, B.Y., Pyun, B.Y., Hong, S.J., 2014. Humidifier disinfectant-associated children's interstitial lung disease. *Am. J. Respir. Crit. Care Med.* 189, 48–56.

Kim, Y.S., Lee, S.B., Lim, C.H., 2017. Effects of didecylmethylammonium chloride (DDAC) on Sprague-Dawley rats after 13 weeks on inhalation exposure. *Toxicol. Res.* 33, 7–14.

Lee, J.H., Kim, Y.H., Kwon, J.H., 2012. Fatal misuse of humidifier disinfectants in Korea: importance of Chemicals in Consumer Products. *Environ. Sci. Technol.* 46, 2498–2500.

Leem, J.H., Lee, J.H., 2017. Humidifier disinfectant-associated specific diseases should be called together as “humidifier disinfectant syndrome”. *Environ. Health Toxicol.* 32, e2017017.

Leverrier, Y., Lorenzi, R., Blundell, M.P., Brickell, P., Kinnon, C., Ridley, A.J., Thrasher, A.J., 2001. Cutting edge: the Wiskott-Aldrich syndrome protein is required for efficient phagocytosis of apoptotic cells. *J. Immunol.* 166, 4831–4834.

Li, X., Song, N., Wang, D., Han, X., Lv, Q., Ouyang, H., Li, Z., 2015. Isoform-specific imprinting of the MEST gene in porcine parthenogenetic fetuses. *Gene* 558, 287–290.

Lim, D.G., 2004. Oxidative stress; reactive oxygen species and nitric oxide. *Korean J. Crit. Care Med.* 19, 81–85.

Lin, H., Liu, S., Gao, W., Liu, H., 2020. DDIT3 modulates cancer stemness in gastric cancer by directly regulating CEBPβ. *J. Pharm. Pharmacol.* 72 (6), 807–815.

Lu, D., Abulimiti, A., Wu, T., Abudureyim, A., Li, N., 2018. Pulmonary surfactant-associated proteins and inflammatory factors in obstructive sleep apnea. *Sleep Breath.* 22, 99–107.

Meta, S.K., Bhasin, K.K., Chauhan, R., Dham, S., 2005. Effect of temperature on critical micelle concentration and thermodynamic behavior of dodecylmethylammonium bromide and dodecyltrimethylammonium chloride in aqueous media. *Colloids Surf. A Physicochem. Eng. Asp.* 255, 153–157.

Naiel, S., Tat, V., Padwal, M., Vierhout, M., Mekhael, O., Yousof, T., Ayoub, A., Abed, S., Dvorkin-Gheva, A., Ask, K., 2019. Protein Misfolding and endoplasmic reticulum stress in chronic lung disease: will cell-specific targeting be the key to the cure? *Chest* 157, 1207–1220.

Ohnuma, A., Yoshida, T., Tajima, H., Fukuyama, T., Hayashi, K., Yamaguchi, S., Ohtsuka, R., Sasaki, J., Fukumori, J., Tomita, M., Kojima, S., Takahashi, N., Takeuchi, Y., Kuwahara, M., Takeda, M., Kosaka, T., Nakashima, N., Harada, T., 2010. Didecylmethylammonium chloride induces pulmonary inflammation and fibrosis in mice. *Exp. Toxicol. Pathol.* 62, 643–651.

- Pamarthy, S., Kulshrestha, A., Katara, G.K., Beaman, K.D., 2018. The curious case of vacuolar ATPase: regulation of signaling pathways. *Mol. Cancer* 17, 41.
- Park, E.J., Seong, E., 2020. Methylisothiazolinone induces apoptotic cell death via matrix metalloproteinase activation in human bronchial epithelial cells. *Toxicol. in Vitro* 62, 104661.
- Park, E.J., Park, S.J., Kim, S., Lee, K., Chang, J., 2018. Lung fibroblasts may play an important role in clearing apoptotic bodies of bronchial epithelial cells generated by exposure to PHMG-P-containing solution. *Toxicol. Lett.* 286, 108–119.
- Park, E.J., Han, J.S., Seong, E., Park, E.J., Lee, B.S., Lee, S.J., Lee, K., 2020. Inhaled Kathon may induce eosinophilia-mediated disease in the lung. *Environ. Toxicol.* 35, 27–36.
- Pubchem, 2005. Didecyldimethylammonium Chloride (Compound). <https://pubchem.ncbi.nlm.nih.gov/compound/Didecyldimethylammonium-chloride/> (accessed 18 May 2020).
- Puleston, D., 2015. Detection of Mitochondrial Mass, Damage, and Reactive Oxygen Species by Flow Cytometry. 2015 Cold Spring Harb. Protoc (pdb.prot086298).
- Reichow, S.L., Hamma, T., Ferré-D'Amaré, A.R., Varani, G., 2007. The structure and function of small nucleolar ribonucleoproteins. *Nucleic Acids Res.* 35, 1452–1464.
- Reynier, M., Allart, S., Gaspard, E., Moga, A., Goudounèche, D., Serre, G., Simon, M., Leprince, C., 2016. Rab11a is essential for lamellar body biogenesis in the human epidermis. *J. Invest. Dermatol.* 136, 1199–1209.
- Rock, K.L., Kono, H., 2008. The inflammatory response to cell death. *Annu. Rev. Pathol.* 3, 99–126.
- Roszell, B.R., Tao, J.Q., Yu, K.J., Huang, S., Bates, S.R., 2012. Characterization of the Niemann-Pick C pathway in alveolar type II cells and lamellar bodies of the lung. *Am. J. Phys. Lung Cell. Mol. Phys.* 302, L919–L932.
- Rovere-Querini, P., Brunelli, S., Clementi, E., Manfredi, A.A., 2008. Cell death: tipping the balance of autoimmunity and tissue repair. *Curr. Pharm. Des.* 14, 269–277.
- Schuck, S., Honsho, M., Ekroos, K., Shevchenko, A., Simons, K., 2003. Resistance of cell membranes to different detergents. *Proc. Natl. Acad. Sci. U. S. A.* 100, 5795–5800.
- Shane, H.L., Lukomska, E., Kashon, M.L., Anderson, S.E., 2019. Topical application of the quaternary ammonium compound didecyldimethylammonium chloride activates type 2 innate lymphoid cells and initiates a mixed-type allergic response. *Toxicol. Sci.* 168, 508–518.
- U.S. EPA, 2005. Guidelines for Carcinogen Risk Assessment. https://www.epa.gov/sites/production/files/2013-09/documents/cancer_guidelines_final_3-25-05.pdf (accessed 18 May 2020).
- U.S. EPA, 2006. Didecyl Dimethyl Ammonium Chloride (DDAC) Risk Assessment (DP Barcode 069149). <http://pi.ace.orst.edu/search/getDocketDocument.s?document=EPA-HQ-OPP-2006-0338-0019> (accessed 18 May 2020).
- Uhlirarova, B., Kopincova, J., Adamkov, M., Svec, M., Calkovska, A., 2016. Surfactant proteins A and D are related to severity of the disease, pathogenic bacteria and comorbidity in patients with chronic rhinosinusitis with and without nasal polyps. *Clin. Otolaryngol.* 41, 249–258.
- Wang, X., Bi, Z., Chu, W., Wan, Y., 2005. IL-1 receptor antagonist attenuates MAP kinase/AP-1 activation and MMP1 expression in UVA-irradiated human fibroblasts induced by culture medium from UVB-irradiated human skin keratinocytes. *Int. J. Mol. Med.* 16, 1117–1124.
- Weaver, T.F., Na, C.L., Stahlman, M., 2002. Biogenesis of lamellar bodies, lysosome-related organelles involved in storage and secretion of pulmonary surfactant. *Semin. Cell Dev. Biol.* 13, 263–270.
- Westman, J., Grinstein, S., Marques, P.E., 2020. Phagocytosis of necrotic debris at sites of injury and inflammation. *Front. Immunol.* 10, 3030.
- Xu, Q., Nakajima, M., Ichikawa, S., Nakamura, N., Roy, P., Okadome, H., Shiina, T., 2009. Effects of surfactant and electrolyte concentrations on bubble formation and stabilization. *J. Colloid Interface Sci.* 332, 208–214.
- Yamano, G., Funahashi, H., Kawanami, O., Zhao, L.X., Ban, N., Uchida, Y., Morohoshi, T., Ogawa, J., Shioda, S., Inagaki, N., 2001. ABCA3 is a lamellar body membrane protein in human lung alveolar type II cells. *FEBS Lett.* 508, 221–225.
- Yoshimatsu, T., Hiyama, K., 2007. Mechanism of the action of didecyldimethylammonium chloride (DDAC) against *Escherichia coli* and morphological changes of the cells. *Biocontrol Sci.* 12, 93–99.
- Zhang, C., Cui, F., Zeng, G.M., Jiang, M., Yang, Z.Z., Yu, Z.G., Zhu, M.Y., Shen, L.Q., 2015. Quaternary ammonium compounds (QACs): a review on occurrence, fate and toxicity in the environment. *Sci. Total Environ.* 518–519, 352–362.